The Gonzaga Journal of Mathematical Sciences

Volume III, Number 1

Fall, 2017

Founder & Managing Editor

Richard Cangelosi
Department of Mathematics
Gonzaga University
Spokane, WA

Contributing Authors
Eli Dawson
Bailey A. Englin
Taha F. Hakkani
Joseph B. Kincanon
Matthew V. Krick
Elijah Michaelson
Lydia E. Pane

Published by the **Department of Mathematics**
Gonzaga University · 502 E. Boone Avenue · Spokane, WA 99258

In This Issue

Biographies of Contributing Authors

Eli Dawson is a Mechanical Engineering major at Gonzaga University on pace to graduate in May 2018. Upon graduation, Eli plans to attend graduate school to pursue a Master's of Science in Mechanical Engineering. His curiosity with the mathematical treatment of non-linear phenomena lead him to investigate the chaotic dynamics of the double pendulum. Consistent with his engineering perspective, Eli provides many visual aids to complement his analysis. Eli grew up in Palo Alto, California and enjoys traveling through the great outdoors. He claims that he will never turn down a game of basketball.

Bailey A. Englin Bailey Englin is a senior pursuing a Bachelor of Science in Mathematics with a minor in economics. She is from Issaquah, Washington where she was born and moved back to after living in Reno, Nevada for ten years. In her free time from school, she works at Costco and works as a student researcher for Vesta Coufal at Gonzaga University, and also loves spending time with her family. Bailey is hoping to find a job upon graduation which utilizes mathematics and economics, possibly in the healthcare field. She is also considering staying within the Costco company and working in their corporate office. Bailey believes that mathematics provides a bridge between all cultures and regions of the world. She views it as a universal tool for solving some of the most challenging puzzles in our society, having applications inside and outside of the mathematical world.

Taha F. Hakkani Taha Hakkani is a junior who is pursuing a Bachelor of Science in Mathematics and Computer Science. He enjoys physical activities such as running, biking and jui-jitsu (of which he has only taken three and a half classes). He is a native of Spokane and he is ready to leave. Born in 1996, he is classified by non-millennials as a millennial. When Taha grows up he wants to be a comedian, but for now he gets his kicks by writing excessively facetious biographies of himself. He is committed to spreading the word that people who like math are cool too.

Joseph B. Kincanon is a senior at Gonzaga University, working on a Bachelor of Science in Economics with minors in Mathematics and (hopefully) Philosophy. The survey economics class he took while in high school was his first exposure to the subject and, like his parents predicted, fell in love with the topic. What he likes the most about the subject is how it ties together so many disciplines, such as history, psychology, and sociology. The fields of behavioral economics, game theory, and development economics are of particular interest to him. After graduating, he plans on pursuing a PhD in Economics and following his father's footsteps in becoming a professor. His only other life goal at the moment is to find the world's best macaroni and cheese.

Matthew V. Krick is a senior mathematics major from Tacoma, Washington. Initially beginning university as a civil engineering major, he began his pursuit in mathematics in 2016. During his free time, he enjoys playing ultimate frisbee, tutoring mathematics at the local community college, and noodling around on guitar. He hopes to become an educator in the future, and spread his passion and appreciation for mathematics to the next generation.

Elijah Michaelson is a senior majoring in Computer Science with a minor in Mathematics. He is planning on pursuing graduate studies in artificial intelligence and machine learning. His hope is that he can use this emerging field of study to better understand how the human brain achieves creative, intelligent action. Additionally, he believes this technology has the potential to make a meaningful impact on the quality of life for current and future generations. Elijah is also passionate about traveling to experience new places, people, and cultures. Coming from Colville, Washington, he enjoys camping and exploring the outdoors.

Lydia Pane is a Senior pursuing a Bachelor of Science in Mathematics with a minor in Chemistry. She is from Longmont, CO and is passionate about the outdoors. Lydia will be applying for Physical Therapy school this next year and plans to incorporate her undergraduate education into her future studies as a physical therapist. She enjoys drawing connections between different fields of study and taking an array of classes from different subjects. This is her first exposure with working on a viral dynamics model, but finds immunology to be a fascinating subject in which she plans to further explore.

Editor's Note

Welcome to the *The Gonzaga Journal of Mathematical Sciences*. This Journal was created to provide a medium through which Gonzaga undergraduates can showcase their research experiences with others within the Gonzaga community. All submissions are reviewed by at least two students and the managing editor. The criteria for publication are:

- submissions must contain a significant mathematical component;
- student authors must engage in a novel exploration (see below);
- submissions must conform to general standards for academic writing.

This issue features contributions from students enrolled in *Nonlinear Ordinary Differential Equations*, Math 452, during the Fall 2017 semester. The course provides an introduction to elementary techniques used in the analysis of nonlinear systems including: the geometry of phase space, linear stability analysis, bifurcation theory, energy and pseudo-energy methods such as Lyapunov functions, the

Poicaré-Bendixson theorem, Liénard systems, chaos theory, the structure of strange attractors, and more.

Students were asked to select a published peer-reviewed journal article on any topic of interest as long as the article focused on the analysis of a system of nonlinear ordinary differential equations. Students were tasked with reproducing as much of the article's results as possible. At a minimum, student were to describe in detail the model and its parameters, write the model in dimensionless form, find all fixed points and perform a linear analysis of those points. Students were then asked to solve the system numerically and interpreted their results with the aid of software packages such as pplane, Mathematica, or Python.

To add a novel element to their analysis, students were asked to pose and explore one or more, "What If?" type questions. The activity requires students to draw upon their personal creativity and problem solving skills. It also provides students with an avenue through which they may experience a sense of discovery as they proceed with their analysis. This novel component is included in a "Further Analysis" section of their articles.

Biological systems provide a rich source of nonlinear phenomena. In this area Lydia Pane examines a highly nonlinear continuous time model for viral dynamics and its application to oncology. Taha Hakkani explores circadian rhythms via coupled oscillators and compares theoretical predictions to pooled data of test subjects in a sleep pattern experiment, and Elijah Michaelson examines a model for a genetic toggle switch to gain insight into the implementation details of cell-fate decision processes.

Two articles in this issue relate to economic theory. Bailey Englin examines the use of the forced van der Pol oscillator to model nonlinear aspects of the business cycle. Joseph Kincanon and Matthew Krick collaborate to examine the dynamics of a two-dimensional map proposed by economist Tõnu Puu as a discrete time model for duopoly pricing.

In the physical sciences, Eli Dawson studies the chaotic behavior of the double pendulum. In addition to investigating mathematical aspects of the model, Mr. Dawson constructed a physical model of the double pendulum, which was then used to test theoretical predictions with numeric simulations and observation.

Richard Cangelosi

December 15, 2017

The Chaotic Behavior of the Double Pendulum

Eli Dawson
Gonzaga University
Department of Mechanical Engineering
edawson@zagmail.gonzaga.edu

Abstract

In this study we will derive and explore the equations of motion for a double pendulum. We begin with a derivation based upon an energy analysis of the Lagrangian for the system and then compare this with equations obtained by a free-body analysis. For certain values of the parameters, the double pendulum exhibits chaotic motion. A simulation is given showing the effect of initial conditions on a system when in its chaotic regime. As part of this study we will examine a physical model of the double pendulum to compare theoretical results with physical data.

1. Introduction

The double pendulum is a classic and demonstrable application of nonlinear dynamics and the idea of chaos. In what appears to be simple harmonic swings for trajectories with a small initial angular displacement, a sudden and seemingly unexplainable change in its motion is observed for trajectories with a larger initial angular displacement. The double pendulum is an excellent place to begin an exploration into nonlinear dynamics.

The pendulum can be modeled in a number of ways, some being whether or not the two pendulums are compound or simple, and how many planes they are allowed to move in. The most classic set-up takes the pendulums as compound and restricted to two-planes, and therefore is considered a two-degrees of freedom system. The governing equations of motion for this typical setup results in two second-order, coupled, ordinary differential equations.

Significant work has been done on the double pendulum (and the triple and the quadruple!), with the term first used by Hugh Blackburn [3] in the 1890's. He created what is now known as the Blackburn Pendulum, or a Harmonograph.

Since then, what we know today as the double pendulum has been analyzed in many different ways, most vigorously for its easy relation to demonstrating chaos in simple systems. A study by [1], develops the equations of motions for the pendulum using Lagrangians, and then takes a look at its various energy surfaces. Other modes of characterizing double pendulum chaos has been done using Lyapunov Exponents [2] and Poincaré Plots [7].

2. Mathematical Models

The mathematical model for the double pendulum consists of two second-order, coupled, ordinary differential equations. There are plenty of ways to obtain the equations of motion for the double pendulum, with the most common being the Langrangian approach. Additionally, using a free-body and force-summing analysis of the system is an option too, and we will see a comparison of the two techniques here. The variables that the system relies on are its angular position, velocity, and acceleration, while the model also contains five parameters. Point masses and rigid/massless connection assumptions are made. A schematic of the system and the model's variables and parameters are given below.

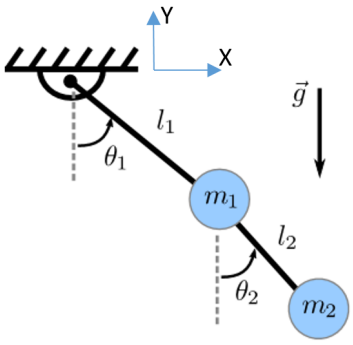

Figure 1: *A planar lumped-mass ideal double-pendulum.*

$\theta_1 =$ The angular position of the top pendulum (radians)
$\theta_2 =$ The angular position of the bottom pendulum with respect to the top pendulum
$\dot{\theta}_1 =$ The angular velocity of the top pendulum
$\dot{\theta}_2 =$ The angular velocity of the bottom pendulum
$\ddot{\theta}_1 =$ The angular acceleration of the top pendulum
$\ddot{\theta}_2 =$ The angular acceleration of the bottom pendulum
$\ell_1 =$ The length of the top pendulum
$\ell_2 =$ The length of the bottom pendulum
$m_1 =$ The mass of the bottom pendulum
$m_2 =$ The mass of the bottom pendulum
$g =$ The acceleration of gravity

2.1. Lagrangian Model

The most common approach in solving the equations of motion is through Lagrangians. They are formed by doing a kinetic and potential energy analysis of the system in order to obtain $L = T - V$, where $T =$ kinetic energy and $P =$ potential energy. We start by solving for x and y, which represent the two degrees of freedom, θ_1 and θ_2.

$$x_1 = \ell_1 \sin\theta_1 \tag{1}$$
$$y_1 = -\ell_1 \cos\theta_1 \tag{2}$$
$$x_2 = \ell_1 \sin\theta_1 + \ell_2 \sin\theta_2 \tag{3}$$
$$y_2 = \ell_1 \cos\theta_1 + \ell_2 \cos\theta_2 \tag{4}$$

We now solve for the Lagrangian $L = T - V$

$$V = m_1 g y_1 + m_2 g y_2$$
$$T = \frac{1}{2} m_1 v_1^2 + \frac{1}{2} m_2 v_2^2$$

Substituting in equations (1),(2),(3), and (4) and solving for $\dot{x_1}$ and $\dot{y_1}$ to use as v_1 and v_2 we obtain

$$V = -(m_1 + m_2)g\ell_1 \cos\theta_1 - m_2 g\ell_2 \cos\theta_2 \tag{5}$$

$$T = \frac{1}{2}m_1\ell_1^2\dot{\theta_1}^2 + \frac{1}{2}m_2(\ell_1^2\dot{\theta_1}^2 + \ell_2^2\dot{\theta_2}^2 + 2\ell_1\ell_2\dot{\theta_1}\dot{\theta_2}\cos(\theta_1 - \theta_2)) \tag{6}$$

To simplify Equations (5) and (6) we introduce

$$\mu = \frac{m_2}{m_1} \qquad \ell = \frac{\ell_2}{\ell_1}$$

Substituting the non-dimensionalized parameters we arrive at the traditional kinetic and potential Lagrangian Equations for the Double Pendulum.

$$T/M_1\ell_1^2 = \frac{1}{2}(1+\mu)\dot{\theta}_1^2 + \mu\ell\cos(\theta_2)\dot{\theta}_1(\dot{\theta}_1 + \dot{\theta}_2) + \frac{1}{2}\mu\ell^2(\dot{\theta}_1 + \dot{\theta}_2)^2 \tag{7}$$

$$V/M_1 g\ell_1 = (1+\mu)(1 - \cos\theta_1 + \mu\ell(1 - \cos(\theta_1 + \theta_2)). \tag{8}$$

We now combine (5) and (6) together with $L = T - V$ to obtain

$$\begin{aligned} L = {} & \frac{1}{2}m_1\ell_1^2\dot{\theta_1}^2 + \frac{1}{2}m_2(\ell_1^2\dot{\theta_1}^2 + \ell_2^2\dot{\theta_2}^2 + 2\ell_1\ell_2\dot{\theta_1}\dot{\theta_2}\cos(\theta_1 - \theta_2)) \\ & + (m_1 + m_2)g\ell_1\cos\theta_1 + m_2 g\ell_2\cos\theta_2 \end{aligned} \tag{9}$$

This is the traditional format of the Lagrangian, and it can now be used to obtain the same equations of motion provided in section 2.2.

2.2. The Free-Body Model

A more tedious way of obtaining the equations of motion is by creating a free-body-diagram of the double pendulum system, and summing forces. We omit the details and give the equations of motion, which are given based on the same parameters and variables discussed in 2.1.

$$\begin{aligned} (m_1 + m_2)\ell_1^2\ddot{\theta_1} + m_2\ell_1\ell_2\cos(\theta_1 - \theta_2)\ddot{\theta_2} + m_2\ell_1\ell_2\sin(\theta_1 - \theta_2)\dot{\theta_2}^2 \\ + (m_1 + m_2)g\ell_1\sin\theta_1 = 0 \end{aligned} \tag{10}$$

and

$$\begin{aligned} m_2\ell_1\ell_2\cos(\theta_1 - \theta_2)\ddot{\theta_1} + m_2 l_2^2\ddot{\theta_2} - m_2\ell_1\ell_2\cos(\theta_1 - \theta_2)\dot{\theta_1}^2 \\ + m_2 g\ell_2\theta_2 = 0 \end{aligned} \tag{11}$$

These are the two second-order, coupled, ordinary differential equations mentioned previously, which could also be obtained from the Lagragian Equations in 2.1.

2.3. State-Space Model

A useful way of looking at these equations is in state-space. If one were to graph the equations of motion in a program such as MATLAB or Mathematica, it is easiest done with functions that take state-space inputs. To get to the very generalized state-space matrix, first a little non-dimensionalizing will help.

We introduce the dimensionless quantities

$$\mu = \frac{m_2}{m_1}, \qquad \ell = \frac{\ell_2}{\ell_1}, \qquad \text{and} \qquad \tau = \sqrt{g/\ell_1}t. \tag{12}$$

We substitute these in Equations (10) and (11) and along with some rearrangement we obtain

$$\begin{aligned}(1+\mu)\frac{d^2\theta_1}{d\tau^2} + \mu\ell\left(\frac{d^2\theta_2}{d\tau^2}\cos(\theta_2-\theta_1) - \left(\frac{d\theta_2}{d\tau}\right)^2\sin(\theta_2-\theta_1)\right) \\ + (1+\mu)\sin\theta_1 = 0\end{aligned} \tag{13}$$

and

$$\mu\ell\left(\frac{d^2\theta_2}{d\tau^2} + \frac{d^2\theta_1}{d\tau^2}\cos(\theta_2-\theta_1) + \left(\frac{d\theta_1}{d\tau}\right)^2\sin(\theta_2-\theta_1) + \sin\theta_2\right) = 0 \tag{14}$$

These equations can be decoupled to obtain one equation containing $\frac{d^2\theta_1}{d\tau^2}$ and another with $\frac{d^2\theta_2}{d\tau^2}$, which can then be entered into the matrix form

$$\begin{bmatrix}(1+\mu) & \mu\lambda\cos(\theta_1-\theta_2)\\ \mu\lambda\cos(\theta_1-\theta_2) & \mu\lambda^2\end{bmatrix}\begin{bmatrix}\frac{d^2\theta_1}{d\tau^2}\\ \frac{d^2\theta_2}{d\tau^2}\end{bmatrix} = \begin{bmatrix}g_1\\ g_2\end{bmatrix} \tag{15}$$

where

$$g_1 = -(1+\mu)\sin\theta_1 - \mu\lambda\left(\frac{d\theta_2}{d\tau}\right)^2\sin(\theta_1-\theta_2),$$

$$g_2 = -\mu\lambda\left(\sin\theta_2 + \left(\frac{d\theta_1}{d\tau}\right)^2\sin(\theta_1-\theta_2)\right).$$

The first matrix (M_1) in (15) is invertible and symmetric, so we can solve for the second derivatives to get

$$\begin{bmatrix}\frac{d^2\theta_1}{d\tau^2}\\ \frac{d^2\theta_2}{d\tau^2}\end{bmatrix} = \frac{1}{det(M_1)}\begin{bmatrix}\mu\lambda^2 & -\mu\lambda\cos(\theta_1-\theta_2)\\ -\mu\lambda\cos(\theta_1-\theta_2) & (1+\mu)\end{bmatrix}\begin{bmatrix}g_1\\ g_2\end{bmatrix}. \tag{16}$$

Equation (16) can then be decoupled into four linearly-independent first-order differentials by introducing the state variables

$$y_1 = \theta_1, \qquad y_2 = \frac{d\theta_1}{d\tau}, \qquad y_3 = \theta_2, \qquad \text{and} \qquad y_4 = \frac{d\theta_2}{d\tau}.$$

A state-space matrix can then be formed with the first-order equations, and that is what is used as input in programs such as MATLAB.

3. Results

By forming the Lagrangian to solve the equations of motion (7) and (8), we have opened up the possibility to take a look at various energy related facets of the equations. One of the things that we will take a look at is the Hamiltonian that can be formed from the Lagrangian, and how this Hamiltonian can be used to graph equipotentials for various setups. Additionally, we will take a look at a proposed numeric scenario that depicts the chaotic nature of the double pendulums equations of motion.

3.1. The Hamiltonian

For a closed system, a Hamiltonian is the sum of the kinetic and potential energy in a system. It is indexed to the frame of reference for the system by a set of canonical coordinates $r = (q, p)$, which represent the Cartesian and Momenta coordinates. The time evolution of the system is described as follows.

$$\frac{dp}{dt} = -\frac{\partial H}{\partial q} \quad \text{and} \quad \frac{dq}{dt} = +\frac{\partial H}{\partial p}. \tag{17}$$

To arrive at the Hamiltonian for the double pendulum, we start at equations (7) and (8) and introduce new dimensionless variables that include the total angular momentum [L], energy [E], and the strength of gravity relative to the total energy [γ] of the system.

We introduce the dimensionless variables

$$t \to t\sqrt{E/m_1\ell_1^2}, \qquad \lambda_i = L_i/\sqrt{Em_1\ell_1^2}, \qquad \text{and} \qquad \gamma = m_1 g\ell_1/E. \tag{18}$$

From (9) we can then obtain the angular momenta $L_i = \frac{\partial T}{\partial \dot{\theta}_i}$

$$L_1/m_1\ell_1^2 = (1 + \mu + 2\mu\ell\cos\theta_2 + \mu\ell^2)\dot{\theta_1} + \mu\ell(\ell + \cos\theta_2)\dot{\theta_2} \tag{19}$$

$$L_2/m_1\ell_1^2 = \mu\ell(\ell + \cos\theta_2)\dot{\theta_1} + \mu\ell^2\dot{\theta_2} \tag{20}$$

Which allows us to solve for the Hamiltonian $h = \frac{T+V}{E}$

$$h = \frac{1}{1+\mu\sin^2\theta_2}\left(\frac{1}{2}\lambda_1^2 - \frac{\ell+\cos\theta_2}{\ell}\lambda_1\lambda_2 + \frac{1+\mu+2\mu\ell\cos\theta_2+\mu\ell^2}{2\mu\ell^2}\lambda_2^2\right) \quad (21)$$
$$+\gamma\{(1+\mu)(1-\cos\theta_1)+\mu\ell[1-\cos(\theta_1+\theta_2)]\}$$

The Hamiltonian shows that the physics of the double pendulum depends on the parameters μ, ℓ, and γ. From the energy conservation depicted in this ideal system, both the Hamiltonian and the equations of motion describe a motion on the three-dimensional energy surface $h = 1$ in four-dimensional space. $(\theta_1, \lambda_1, \theta_2, \lambda_2)$

3.2. Equipotentials

An equipotential is a helpful tool for looking at energy affiliations within the model. For the scenario presented in Figure 2, the angle θ_1 is the displacement of the mass m_1 measured counterclockwise from the negative y-axis, while θ_2 is the displacement of m_2 measured counterclockwise counterclockwise relative to the axis described by θ_1. From the three cases presented below, a few observations are made. The potential will assume its minimum value of zero when $\theta_1 = \theta_2 = 0$. Saddle points of the potential will occur when $\theta_2 = \pi$ if $\theta_1 = 0$ or $\theta_1 = \pi$. The greatest potential will occur at $\theta_1 = \pi$ while $\theta_2 = 0$. From the second figure, the saddles will then become degenerate when the center of gravity for $\theta_2 = \pi$ coincides with the suspension point, $\ell = (1+\mu)/\mu$. As the length ratios are increased past ℓ_2, the nodes are no longer degenerate, however they begin to shift counter-clockwise and depict angle restrictions $\theta_{1,2} < \pi$ when the potential energy exceeds the total energy (E) at the lower saddle point.

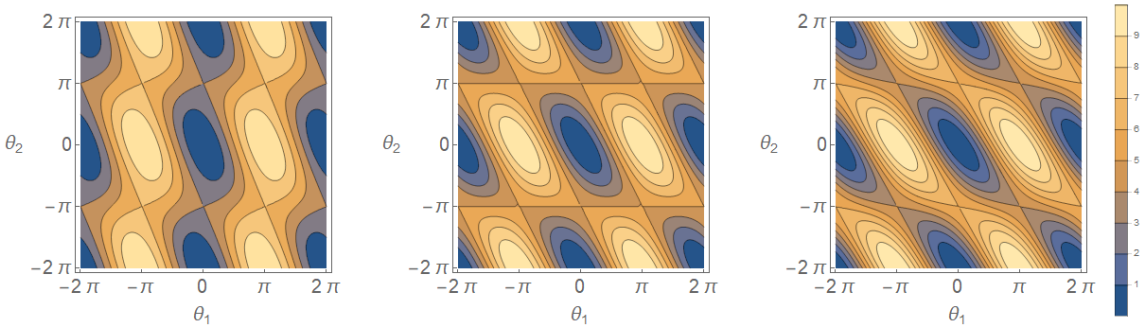

Figure 2: *Equipotential lines V/(γE)=1,2,3... (as indicated by color) for equal masses μ=1 and length ratios ℓ=1 (left), ℓ=2 (center), and ℓ=3 (right)*

3.3. Sensitivity to Initial Conditions

In relation to chaos, the dependence on initial conditions can be easily seen in a double pendulum simulation. By creating a MATLAB script using the ODE45 function that takes a decoupled state-space matrix input described in Section 2.3, a numerical simulation is presented in Figure 3 (thanks to Dr. Timothy Fitzgerald).

The following parameters of the system are used:

Quantity	Value
$m_1 g$	1.0 lb
$m_2 g$	2.0 lb
ℓ_1	18.0 in
ℓ_2	9.0 in

Two initial conditions are explored for these parameters:

$$(a) \qquad \theta_1(0) = 90^\circ, \quad \theta_2(0) = 90.0^\circ, \quad \dot{\theta_1}(0) = 0, \quad \dot{\theta_2}(0) = 0 \tag{22}$$

$$(b) \qquad \theta_1(0) = 90^\circ, \quad \theta_2(0) = 90.1^\circ, \quad \dot{\theta_1}(0) = 0, \quad \dot{\theta_2}(0) = 0 \tag{23}$$

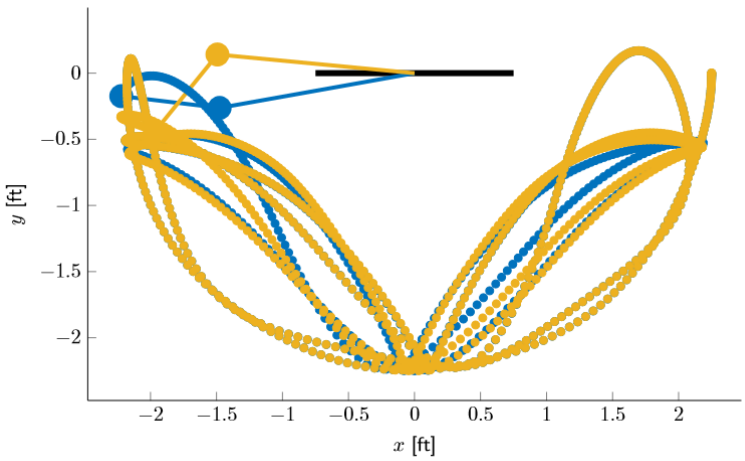

Figure 3: *Double Pendulum Motion for case (a)-blue and (b)-orange for 0 to 6 s.*

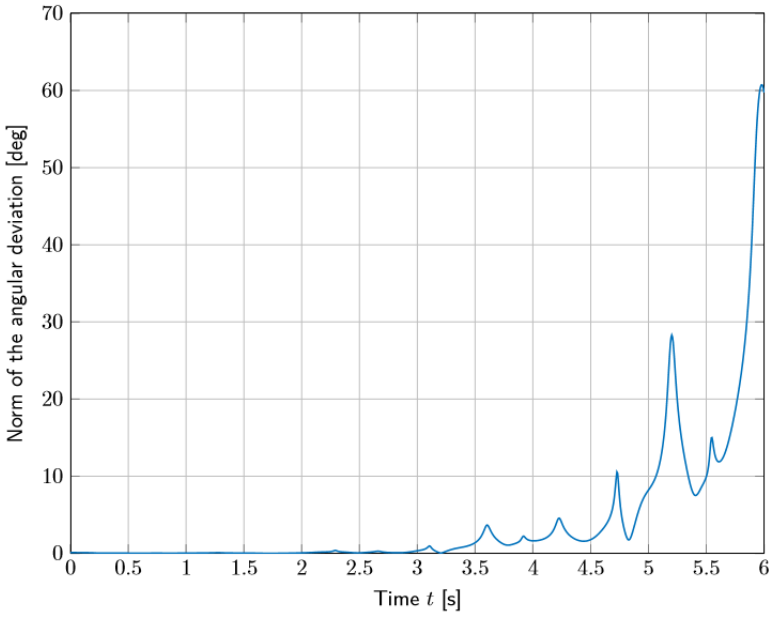

Figure 4: *Double Pendulum Variation for case (a) and (b) for 0 to 6 s.*

From the graphed simulations, it becomes apparent how serious the initial conditions will dictate the motion of the pendulum. After 3 seconds, the two scenarios begin to show a variation in their angles, despite just a 0.1° difference in starting position. As time goes on, these angles begin to deviate even more. As is true with chaos, the long term motion of the system seems to fluctuate greatly. No intuitive relationship can be discerned by just looking at the graphs. This is the beauty of chaos, and how sensitivity to initial conditions make motions become more and more unpredictable as time goes on.

4. Further Analysis

As is true with all principles of mathematics, we can find real world examples that directly use these models to predict and control scenarios. An application of the double pendulum is frequently found in control systems, the most popular of which is called the "inverted double pendulum on a cart". The scenario involves a double pendulum being placed on a slider that can move back and forth on a fixed axis. The idea of this system is that the slider will accelerate very quickly with the pendulums both hanging down at 0°, and then abruptly change its direction of motion several times in a brief instance. By doing this, the system is able to change its angular velocities the requisite amount for the pendulum to reach a stable point directly on top of each other, 180° from where they began.

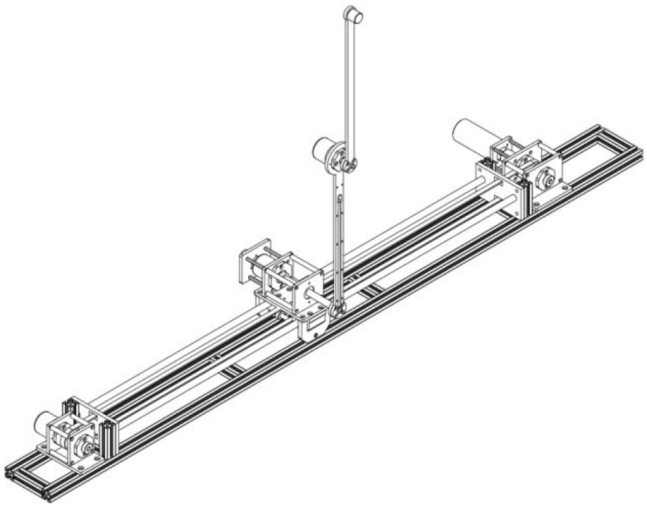

Figure 5: *Inverted Double Pendulum on a Cart*

The ideal equations of motion for this scenario can be found from [6]. However, in reality when these simulations occur, the friction in the pendulum bearings must be accounted for. The reason for this is that the friction allows for what the traditional model predicts as an unstable node to become more stable than predicted, which is why these straight up positions (depicted in Figure 5) are achievable. Similar steps may be taken to arrive at the equations presented in [6] as done in this article, especially forming the Hamiltonian and graphing equipotentials for various parameters. A video of this control problem in action can be found at https://www.youtube.com/watch?v=B6vr1x6KDaY.

Further analysis definitely worth looking into for the double pendulum include Poincaré Plots, finding Lyapunov Exponents, or finding the energy excitation levels needed to cause a "flip" of the pendulums. Something else to consider would be to try and replicate the frictional forces present in the model, and see whether the extra parameters introduced will give a smaller range for what would be considered the chaotic regime.

5. Discussion

The whole idea of this article has been to introduce a system that seems so simple, yet displays a plethora of different behaviors which yields endless options of exploration. With a physical model it becomes a fun exercise to see what kind of conditions we can try to mimic from the ideal model, or how difficult it is to match the predictions for the long-term. With a very basic introduction to the double pendulum, it is the hope of this article to spur some more creative insight

to be developed for this system, or bridge the gap to a more involved scenario such as the inverted double pendulum on a cart as discussed before.

It is an accepted fact that we will never be able to model anything perfectly; however, we still are capable of creating models that would seem flawless to the untrained eye. With a shift into a chaotic regime predictability becomes impossible. Even the untrained eye can tell when something is amiss. Understanding these systems has serious implications in the real world (for example, predicting the weather) and being able to gain an understanding of a very simple model will allow one to understand why real world models are so volatile.

Editor's note. A fine physical model of the double pendulum was built by the author and generously donated by the author to this very appreciative editor.

6. Acknowledgments

A special thanks to Dr. Richard Cangelosi for making this journal a possibility and the countless hours he has spent helping these articles turn from rags to riches. His course on nonlinear differential equations formed the basis for all analysis conducted herein. To the Gonzaga Mathematics Department for allowing a mechanical engineering student to take one of its classes and to Dr. Timothy Fitzgerald for his insight and scenario presented in his Controls Systems class.

References

[1] Arnold, V.I. (1978). *Mathematical Methods of Classical Mechanics.* Springer, Berlin, Heidelberg, New York

[2] Arnold, V.I. (2010). *Graduate Texts in Mathematics: Mathematical Methods of Classical Mechanics, 2. ed.* Springer

[3] Gray I. (2017). Hugh Blackburn (1823 to 1909). In: *Snake Charming - The Musical Python*. Springer, Cham.

[4] Richter, Scholz (1984). *Chaos in Classical Mechanics: The Double Pendulum.* Stochastic Penomena and chaotic behavior in complex systems: proceedings of the fourth meeting of the UNESCO Working Group on Systems Analysis, Fla

[5] Strogatz, Steven H. (2015). *Nonlinear Dynamics and Chaos with Applications to Physics, Biology, Chemistry, and Engineering.* Westview Press: Boulder, CO.

[6] Vorlesungen (2013). *Equations of motion for an inverted double pendulum on a cart (in generalized coordinates).* http://www3.math.tu-berlin.de/Vorlesungen/SS12/Kontrolltheorie/matlab/invertedpendulum.pdf [Accessed 5 Dec. 2017].

[7] Morin, D. (2008). *Introduction to Classical Mechanics: With Problems and Solutions.* Cambridge University Press

The Forced van der Pol Oscillator as an Economic Model for the Nonlinear Accelerator Principle

Bailey English

Gonzaga University
Department of Mathematics
benglin@zagmail.gonzaga.edu

Abstract

In this report we examine a nonlinear model for the business cycle. Following the work of Goodwin (1951), we begin with a standard linear model and then incorporate additional aspects of the business cycle to increase the model's realism. In doing so, we arrive at Goodwin's nonlinear accelerator model, which is readily seen as the unforced van der Pol oscillator. We use standard techniques from dynamical systems theory to analyze the van der Pol oscillator and then extend the model to include constant and periodic forcing. We conclude with an interpretation placing results obtained in a economic context.

1. Introduction

The complex dynamics of economic systems can be studied using mathematical techniques employed in the analysis of nonlinear model. With that in mind, we note that certain models of the business cycle can be reduced to the forced van der Pol oscillator [4, 6, 8, 11]

$$\ddot{u} + \gamma(u^2 - 1)\dot{u} + u = G(t). \tag{1}$$

When the parameter $\gamma >> 1$, Equation (1) is considered part of a broad class of oscillators known as relaxation oscillators.

In 1951, R.M. Goodwin [4] looked at the accelerator and economic cycle theory in a nonlinear way, which previously was analyzed via linear models. The drawback of a linear model is that they do not take into account lags or basic

elements of oscillations. Also, when analyzing them linearly, one will reach the conclusion that the model will either explode or die away, meaning the society essentially disappears, which is clearly not logical. Linear theory also requires that an economic downswing to be the same as the upswing as opposed to nonlinear theory where the depression can be different in form and duration from the boom cycle, which more accurately describes an economy's business cycle.

The accelerator principle [1] is an economic concept that draws a connection between output and capital investment. According to the acceleration principle, if demand for consumer goods increases, then the percentage change in the demand for machines and other investment necessary to make these goods will increase even more (and vice versa). In other words, if income increases, there will be a corresponding but magnified change in investment. The acceleration principle has the effect of exaggerating booms and recessions in the economy. This makes sense, as companies want to optimize their profits when they have a successful product, they begin investing in more factories and capital investments to produce more. If a recession hits, they will reduce investment. This investment reduction can increase the length of the recession. This is because less investment means less jobs created, and so on. The idea of the accelerator principle has been used in economic theory to link output to capital investment since the 1930's.

Since Goodwin's paper was published, other authors have published papers building on the foundations of the model Goodwin presents. Tobin [10] presents a simple aggregative model that allows for the possibility of substitutions and monetary effects. This model has a similar cyclic behavior as Goodwin's, but this cycle depends on the inflexibility of prices, monetary wages, or supply of monetary assets. Chen [3] presents actual empirical and theoretical investigations of chaos in macroeconomic models. While Goodwin's paper presents a theoretical model of the nonlinear accelerator, this paper provides techniques in testing economic aggregate movements. Lorenz and Nusse [7] present Goodwin's model and use it as an economic example of emergence of complex motion in nonlinear dynamical systems.

Goodwin's nonlinear accelerator provided a new foundation for a model that more accurately represents the business cycle. We will look at his series of models that take into account different properties of economies. This will lead to analyzing the final model that he presents that is his nonlinear accelerator. Finally, we will see how this analysis can provide more insights into how nonlinear theory can find applications in macroeconomic theory.

2. Mathematical Model

2.1. Linear Model

Goodwin [1] introduces a basic linear model of the business cycle. The linear consumption function is

$$\xi = ky \tag{2}$$
$$c = \alpha y + \beta \tag{3}$$
$$y = c + \dot{k} \tag{4}$$

where ξ is desired capital stock, y is income, c is consumption, $\dot{k}$ is the rate of change in capital stock, and k, α, and β are all constants. In order to fix one of the simplicities of this model, the fact that multiplication takes time, Goodwin replaces equations (3) and (4) with

$$y = \alpha y + \beta + \dot{k} - \varepsilon\dot{y}. \tag{5}$$

This equation is a multiplier, with a lag introduced by $\varepsilon\dot{y}$. A multiplier is the factor by which the return deriving from an expense exceeds the expense itself. Goodwin presents other equations accounting for technological progress and autonomous and induced investment, but these will not effect his final, expanded model.

2.2. The Nonlinear Expanded Model

The nonlinear model accounts for the lag between decisions to invest and the corresponding outlays, or expenses. Outlays tend to lag behind decisions by approximately one half the length of time required for fabrication [4]. Because of this, we can say

$$O_I(t+\theta) \approx O_D(t) = \varphi[\dot{y}(t)] \tag{6}$$

where O_I is investment outlays, O_D is investment decisions, φ is induced investment and θ is one half the construction time of new equipment. With this, we can rewrite equation (5) as

$$\varepsilon\dot{y}(t+\theta) + (1-\alpha)y(t+\theta) = O_A(t+\theta) + \varphi[\dot{y}(t)] \tag{7}$$

where O_A is the sum of the independent expenses β and l, with β being the historically given upward drift of the consumption function, which expresses consumer spending, and l being the historically given investment expenses. Taking

this equation, we can expand the two leading terms in a Taylor series and then keep only the first two terms in each.

Recall that the Taylor series representation of a function $y = y(\theta)$ about a point t is given by

$$y(\theta) = y(t) + \dot{y}(t)(\theta - t) + \mathcal{O}\left((\theta - t)^2\right). \tag{8}$$

Employing (8) and retaining only first-order terms we have

$$y(t + \theta) = y(t) + \dot{y}(t)(t + \theta - t) = y(t) + \theta\dot{y}. \tag{9}$$

Computing the time derivative of (9) and multiplying by ε yields

$$\varepsilon\dot{y}(t + \theta) = \varepsilon\dot{y} + \varepsilon\theta\ddot{y}. \tag{10}$$

Making use of (9) and (10), we may rewrite (7) as

$$\varepsilon\dot{y} + \varepsilon\theta\ddot{y} + (1 - \alpha)y + (1 - \alpha)\theta\dot{y} - \varphi(\dot{y}) = O_A(t + \theta). \tag{11}$$

This gives us the new, expanded equation.

Now, by shifting our autonomous injections by θ time units and calling it O*, we get

$$\epsilon\theta\ddot{y} + [\epsilon + (1 - \alpha)\theta]\dot{y} - \varphi(\dot{y}) + (1 - \alpha)y = O^*(t)$$

For now, we take $O^*(t)$ to be a constant, O^*. We then look at deviations from the equilibrium income by substituting $z = y - O^*/(1 - \alpha)$ which gives us

$$\epsilon\theta\ddot{z} + [\epsilon + (1 - \alpha)\theta]\dot{z} - \varphi(\dot{z}) + (1 - \alpha)z = 0$$

This equation can then be reduced to a dimensionless form, which Goodwin does in his paper so see [4] for more details on this. This equation in dimensionless form becomes

$$\ddot{x} + [X(\dot{x})/\dot{x}]\dot{x} + x = 0$$

which very closely resembles the well-known van der Pol oscillator [11]. This will be the equation we will be analyzing.

3. Model Analysis: van der Pol Oscillator

The van der Pol oscillator (VDP), given by Equation (1), resembles a simple harmonic oscillator, but with the important difference that it contains a nonlinear damping term $\mu(x^2 - 1)\dot{x}$. The system will eventually become a self-sustained oscillator, where the energy lost over a cycle balances with the energy coming in [9].

To begin analyzing this relaxation oscillator, Strogatz [3] rewrites the system using a Liénard transformation. Equation (12) is a generalization of the van der Pol oscillator and lends itself nicely to a theorem that states that the system has a unique, stable limit cycle under certain hypotheses that the functions f and g must satisfy. This equation can also be written as a system of equations that is helpful for doing a transformation on the van der Pol oscillator to make the analysis easier. The Liénard's equation is

$$\ddot{x} + f(x)\dot{x} + g(x) = 0 \tag{12}$$

which is equivalent to the system

$$\dot{x} = y \tag{13a}$$

$$\dot{y} = -g(x) - f(x)y. \tag{13b}$$

By looking at these equations and the theorem, Strogatz [9] is able to determine multiple results about the van der Pol oscillator. First, by looking at Liénard's Theorem and doing a little bit of analysis, he concludes that the van der Pol oscillator has a unique, stable limit cycle. This limit cycle can be seen in Figure 1. Any initial point we pick in the diagram will immediately shoot to the limit cycle and remain on it. Next, by using the Liénard plane, it makes it much easier to do a phase plane analysis of the VDP oscillator. In Figure 2, we can see the time series of x and y with time, with x being the position and y being the velocity. By doing this transformation, the oscillator becomes the system of equations

$$\dot{x} = \mu[y - F(x)] \tag{14a}$$

$$\dot{y} = \frac{-1}{\mu}x \tag{14b}$$

where

$$F(x) = \frac{1}{3}x^3 - x \tag{15}$$

This transformation makes it easier to see the nullclines and trajectories, as seen in the phase plane in Figure 1.

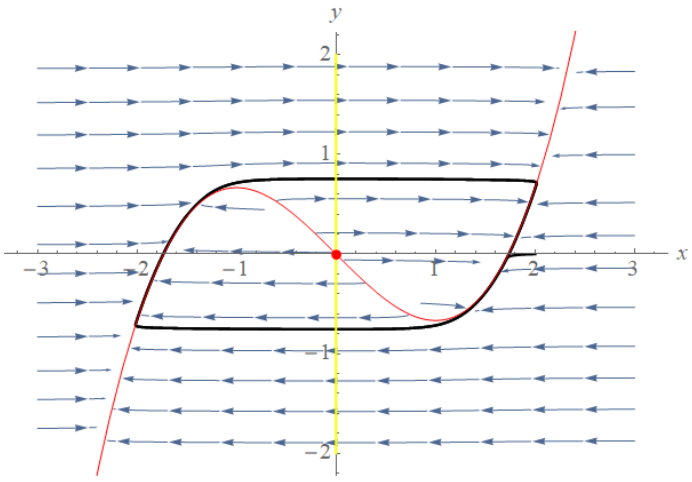

Figure 1: *Phase plane of the unbiased van der Pol oscillator. The x-nullcline is given by the red cubic shaped curve and the y-nullcline is the vertical yellow line. The intersection at the origin is the system's sole fixed point, which is located at the origin. The stable limit cycle is shown in black.*

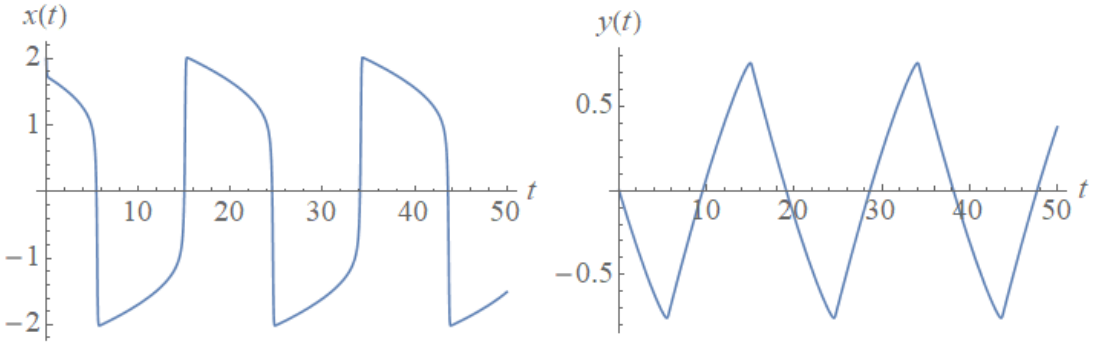

Figure 2: *Time series for the unbiased van der Pol oscillator. Observe in the graph of $x(t)$ the slow initial decline during approximately the first 5 time units followed by a very rapid decline. The oscillator then begins to slowing increase until a threshold is reach at which time a very rapid rise ensues. The rapid increase and decrease correspond to the near horizontal upper and lower boundaries of the limit cycle given in Figure 1. The periods of slow build-up correspond to the left and right boundaries of the limit cycle.*

4. Further Analysis

We will now look at a biased van der Pol oscillator, that is, the van der Pol oscillator subject to a constant external force, and see how the analysis changes. This new equation is

$$\ddot{x} + \mu(x^2 - 1)\dot{x} + x = a \tag{16}$$

where the constant a is some real parameter and $\mu > 0$ as usual.

We first find and classify the fixed points. In order to do this, we will do what we did with the unbiased oscillator and write our system in Liénard form. We will define $F(x)$ so that

$$\ddot{x} + \mu(x^2 - 1)\dot{x} = \frac{d}{dx}(\dot{x} + \mu F(x)) \tag{17}$$

Then, doing the same analysis as in the unbiased case, we find that

$$\dot{y} = \frac{-(x - a)}{\mu} \tag{18}$$

So, our system becomes

$$\dot{x} = \mu[y - F(x)] \tag{19a}$$

$$\dot{y} = -\frac{x - a}{\mu} \tag{19b}$$

From this we can see that our x-nullcline becomes $y = F(x)$ and our y-nullcline becomes $x = a$. The intersection of the nullclines gives our only fixed point at $x^* = (a, F(a)) = (a, a^3/3 - a)$. The phase plane can be seen in Figure 3, where $a = 0.5$. As we can see, it is the same as the phase plane for the unbiased oscillator.

Now that we have our fixed point, our next step is to determine the stability of this point by evaluating the Jacobian matrix at this point to get

$$J_e \equiv J|_{x^*} = \begin{bmatrix} -\mu(a^2 - 1) & \mu \\ -\frac{1}{\mu} & 0 \end{bmatrix}.$$

We see that the trace of J_e is $\tau = -\mu(a^2 - 1)$ and the determinant is $\Delta = 1$. From this we see that the characteristic equation is

$$\sigma^2 + \mu(a^2 - 1)\sigma + 1 = 0 \tag{20}$$

To determine the stability of the fixed point, we use the Routh-Hurwitz criterion. According to the criterion, if the trace, $\tau < 0$ and the determinant $\delta > 0$, then the

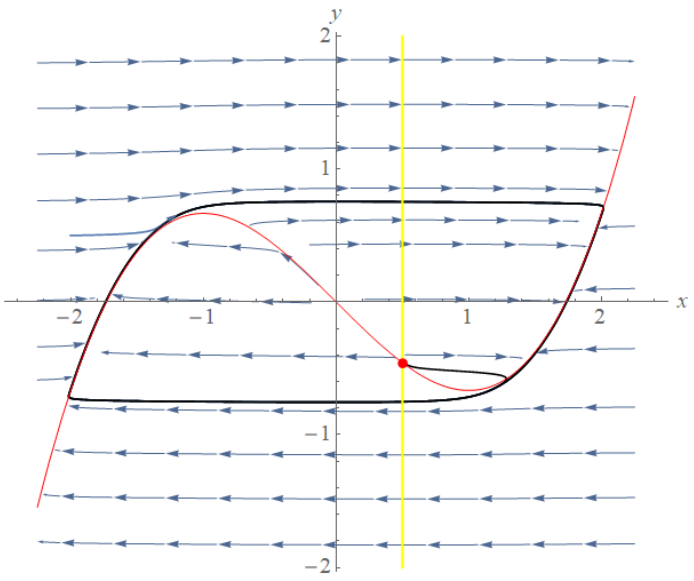

Figure 3: *Phase plane with limit cycle of biased van der Pol oscillator with* $a = 0.5$.

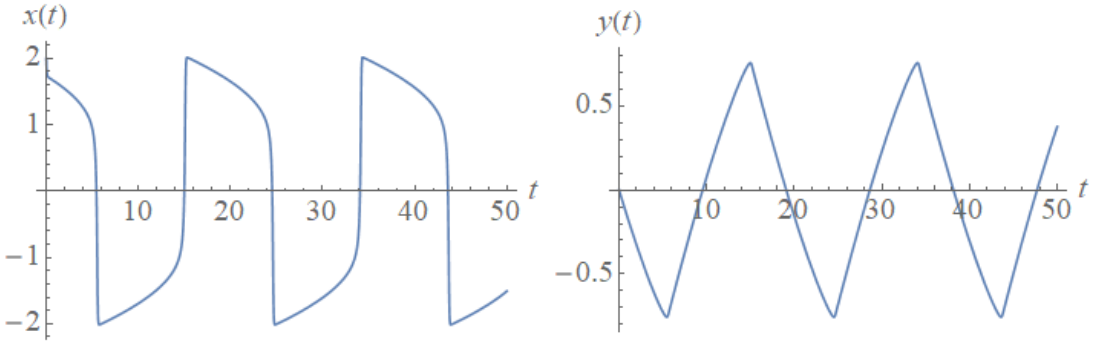

Figure 4: *Time series of biased van der Pol oscillator with* $|a| < 1$.

real part of the eigenvalues are negative. Since our determinant is always 1 and therefore > 0, we need to examine the $\mu(a^2 - 1)$. Looking at this, we can see we will have a bifurcation point at $a = 1$. So, if

$$|a| > 1 \quad \text{then} \quad \mu(a^2 - 1) > 0, \tag{21}$$

and the fixed point is stable, but we have an unstable limit cycle. If

$$|a| < 1 \quad \text{then} \quad \mu(a^2 - 1) < 0, \tag{22}$$

and the fixed point is unstable, but we have a stable limit cycle. The limit cycle of this can be seen in Figure 3, and the time series can be seen in Figure 4. Both of these pictures will look the same as the unbiased oscillator pictures.

5. Economic Relevance

The nonlinear model that Goodwin [4] presents is for an unprogressive economy, meaning income and capital always return to their previous lows and highs and can never improve. Goodwin makes this assumption by setting the oscillator equal to 0. This can be seen graphically when we look at the limit cycle behaviour. The cycle moves from its low point to high point, but it can never break out of this loop. In order to model a more realistic, progressive economy, we need to have the van der Pol oscillator equal to a forcing function. This will alter the stable limit cycle and more accurately portray how an economy will not necessarily return to its previous lows and highs.

6. Future Work

To further extend this project, we could analyze the van der Pol oscillator set equal to not constant forcing function. One such model is given by

$$\ddot{u} + \gamma(u^2 - 1)\dot{u} + u = Acos(\omega t) \tag{23}$$

The system of equations is now

$$\dot{x} = \mu[y - F(x)], \tag{24a}$$

$$\dot{y} = -\frac{1}{\mu}\left[x - A\cos(\omega t)\right]. \tag{24b}$$

This system no longer autonomous because t now appears explicitly. Because of this, we would need to add a new dimension to our systems, now giving us a three dimensional system to be analyzed in the future.

Editor's note. The nonautonomous system given by (24) may be written as

$$\dot{x} = \mu[y - F(x)], \tag{25a}$$

$$\dot{y} = -\frac{1}{\mu}\left[x - A\cos(\omega z)\right], \tag{25b}$$

$$\dot{z} = 1, \tag{25c}$$

where we set $z = t$. Significant progress has been made by [2, 5] and others in understanding the dynamics of Equations (25); however, several open questions remain.

Acknowledgements

I would like to thank Dr. Cangelosi for his contribution to the organization and writing of the Introduction section and for his guidance with the analysis of the models considered in this report.

References

[1] Acceleration principle. BusinessDictionary.com. Retrieved November 21, 2017, from BusinessDictionary.com website: http://www.businessdictionary.com/definition/acceleration-principle.html

[2] Bold K, Edwards C, Guckenheimer J, Guharay S, Hoffman K, Hubbard J, Oliva R and Weckesser W., (2003). The forced van der Pol equation II: canards in the reduced system, *SIAM J. Appl. Dyn. Syst.*, **2**, 570-608.

[3] Chen, P., (1988). Empirical and theoretical evidence of economic chaos. *System Dynamics Review,* **4**, 81-108.

[4] Goodwin, R.M., (1951). The nonlinear accelerator and the persistence of business cycles. *Econometrica,* **19**(1), 1-17.

[5] J. Guckenheimer, K. Hoffman, W. Weckesser, (2003). The forced van der Pol equation I: the slow flow and its bifurcations, *SIAM J. Appl. Math. Systems*, **2**, 1-35.

[6] Kaldor, A model of the trade cycle. *Economic J.*, **50**, 78-92.

[7] Lorenz, Hans-Walther and Nusse, Helena. (2002). Chaotic attractors, chaotic saddles, and fractal basin boundaries: Goodwin's nonlinear accelerator model reconsidered. *In Chaos, Solitons and Fractals,* **13**(5), 957-965.

[8] Puu, T. and Sushko, I (2004). A business cycle model with cubic nonlinearity. *Chaos, Solitons & Fractals,* **19**(3), 597 - 612.

[9] Strogatz, Steven, (2015). *Nonlinear Dynamics and Chaos.* Westview Press, 198-243.

[10] Tobin, James. (1955). A dynamic aggregative model. *Journal of Political Economy,* **63**(2), 103-115.

[11] van der Pol, Balthasar. (1926). LXXXVIII. On "relaxation-oscillations." *The London, Edinburgh, and Dublin Philosophical Magazine and Journal of Science*, **2**(11), 978-992.

A Mathematical Analysis of Sleep Cycles and Circadian Rhythms

Taha F. Hakkani

Gonzaga University
Department of Mathematics
thakkani@zagmail.gonzaga.edu

We analyzed the results found when comparing a nonlinear model involving coupled circadian oscillators to pooled data of test subjects in "free-run" sleep patterns. By non-dimensionalizing the model, we were able to determine conditions for which internal and external synchronization would be established. Based on those conditions, linear stability analysis reveals how sleep and circadian phases differ during external synchrony. Because of the simplicity of the model, we were also able to write the phase difference explicitly as function of time, which was used to test the relationship between circadian phase and sleep duration. This model reflected the pooled data well except on one account: timing of sleep onset in relation to circadian phase. We proposed a modification to the original model to correct for this discrepancy.

1. Introduction

That human internal clocks seem to be in sync with the 24-hr day should not be a surprise to anyone. It isn't until we witness those who confine themselves from both daylight and the 24-hour society do we see the steady sleep-wake cycle come undone. How light affects the body's sleep cycles has never been as obvious as it is in this modern age. Blue light emitted from cell phones and television sets can have a serious impact on sleep and health [5]. A deeper understanding of how the body's endogenous cycles interact with each other can be useful for further research on health and lifestyle habits.

Data related to human circadian rhythms can be found in [1, 2, 4]. In an experiment described in [2], Siffre secluded himself in a cave for half a year, with no access to daylight or society. In his 'free-run' experiment, he experienced weeks of normal 24-26 hours sleep-wake cycles interrupted by seemingly random long stretches of sleep. When Cziesler [1] recreated this effect a few years later

the same phenomenon emerged in his test subjects. Cziesler also happened to be monitoring internal body temperatures, hormones, and brain waves. When sleep-wake times were tracked against the circadian temperature cycle, certain patterns emerged. One interesting pattern is that long periods of sleep generally start at temperature peaks, while shorter sleep periods happen at temperature troughs. Also, subjects rarely wake up as temperature is falling. These patterns are so pervasive in external desynchronization that mathematical models of this phenomenon are judged partly on their ability to incorporate them [3].

Due to the periodic nature of sleep, many mathematical models of the interplay between sleep-wake cycles and circadian cycles use a system of coupled oscillators. These models have seen varying degrees of success [3]. One struggle has been that due to their complex non-linear natures, they must be solved numerically. In this article, we will attempt to analyze and reproduce results found in Strogatz [3]; his model is given by Equations (1). In contrast to models proposed in previous years, Equations (1) can be solved exactly, so computer simulations are not needed. We will then suggest a modification to this model and discuss research done in this field since.

2. Mathematical Model

2.1. Motivation

Because we are dealing with periodic processes (namely circadian temperature and sleep-wake cycle), we will imagine that each process operates on a circle. Then each angle θ corresponds to a unique phase of the process. Applying this to the case of circdian body temperature, we will arbitrarily assign $\theta_1 = 0$ to be temperature troughs, and we'll scale its period to 1 (as in 1 'temperature-day'). This would mean that "noon" in temperature-days roughly correspond to temperature peaks (i.e. $\theta_1(max) \approx 0.5$). Similarly, we will define sleep to always begin at $\theta_2 = 0$ and scale its period to 1.

If we were oblivious to the effects of desynchronization on the sleep-wake cycle and circadian temperature, we might be tempted to say that both of these processes always move around their respective circles more or less linearly, like a clock. After all, we usually rise and retire at roughly the same time every day. But it only takes a small perturbation, such as staying up late or changing time zones, to inevitably force the body into breifly lengthening its sleep-wake cycle to compensate.

In more dramatic cases of internal desynchronization, like the one described in [1, 2] sleep cycles were lengthened by a factor of 1.1 - 1.9 for weeks at a time while circadian temperature cycles shortened (i.e. $\dot{\theta}_1$ decreased and $\dot{\theta}_2$ increased);

and when internal synchronization spontaneously returned, sleep cycles would shorten and temperature cycles would lengthen. This inverse relationship between sleep and temperature cycles strongly suggests that each cycle sends feedback into the speed of the other. Further inspection of [1, 4] shows that internal synchronization occurs when the two cycles are in phase, which means that frequencies are influenced by phase *differences*. Hence, we can characterize the circadian temperature cycle and the sleep cycle as a pair of coupled oscillators:

$$\dot{\theta}_1 = \omega_1 - C_1 \cos 2\pi(\theta_2 - \theta_1) \tag{1a}$$

$$\dot{\theta}_2 = \omega_2 + C_2 \cos 2\pi(\theta_1 - \theta_2) \tag{1b}$$

where

$$0 \leq \theta_1,\ \theta_2 < 1 \tag{2}$$

and

$$\omega_1,\ \omega_2,\ C_1,\ C_2 > 0. \tag{3}$$

This is what Strogatz [3] calls the PHASE model.

2.2. Structure

The constants ω_1 and ω_2 represent the preferred frequencies of each oscillator. One way to interpret ω is to imagine that temperature and sleep cycles don't send feedback to each other. Then temperature and sleep would independently oscillate at a constant rate of ω_1 and ω_2, respectively.

C_1 and C_2 reflect how strongly sleep-wake and temperature phases affect the other. For instance, we can see that the *larger* C_1 is, the more the temperature cycle is slowed down from its preferred frequency, and the *larger* C_2 is, the more the sleep wake cycle is sped up. Because C_1 and C_2 affect the feedback term of each equation, we'll call them coupling strengths.

The factor 2π in each feedback term scales the period to 1, which allows us to discuss phases in terms of "days" as opposed to radian angles.

Finally, we turn our attention to the $(\theta_2 - \theta_1)$ and $(\theta_1 - \theta_2)$ expressions. The speed of each oscillator is modified by the difference in phase. Notice that by symmetry of cosine, we can use $(\theta_2 - \theta_1)$ and $(\theta_1 - \theta_2)$ interchangibly. The difference seen in this expression between the two equations is just an artifact of the standard model of coupled oscillators, which uses sine functions instead.

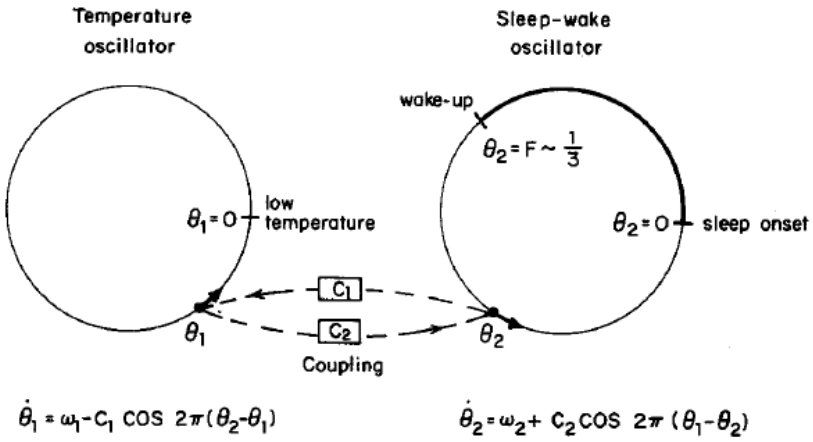

Figure 1: *Temperature lows are defined to be $\theta_1 = 0$. Sleep is defined to be $\theta_2 = 0$. The strength of the feedback from one oscillator to the other is dictated by phase differences and constants C_1 and C_2.*

2.3. Dimensionless Form

It would be nice to have a way to quickly determine how changing parameter values will effect the model's predictions. Writing this model in dimensionless form will allow us to easily identify the parameter relationships that reflect either internal or external synchrony. Because internal synchrony depends strictly on phase difference in externally desynchronized subjects, following [3] let

$$\psi(t) = \theta_1(t) - \theta_2(t) \tag{4}$$

be the phase difference at time t. Then

$$\begin{aligned} \dot{\psi} &= \dot{\theta_1} - \dot{\theta_2} \\ &= (\omega_1 - C_1 \cos 2\pi\psi) - (\omega_2 + C_2 \cos 2\pi\psi) \\ &= \Omega - C \cos 2\pi\psi \end{aligned} \tag{5}$$

where

$$\Omega = \omega_1 - \omega_2 \tag{6}$$

is the difference in preferred frequencies and

$$C = C_1 + C_2 > 0 \tag{7}$$

is the total coupling strength.

Notice that $\dot{\psi} = 0$ has a solution only when $C > |\Omega|$. Now, let's scale time so we are dealing in terms of preferred frequencies. Because Ω has units of frequency,

$$\tau = \Omega t \tag{8}$$

is dimensionless time. Then (5) becomes

$$\frac{d\psi}{d\tau} = 1 - \frac{C}{\Omega}\cos 2\pi\psi. \tag{9}$$

We already determined that we only have fixed points if $C > |\Omega|$. This corresponds to external synchrony. So, we only have synchrony if

$$k = \left|\frac{C}{\Omega}\right| > 1. \tag{10}$$

Since both C and Ω are in units of frequency, $\frac{C}{\Omega}$ is a dimensionless group and our final dimensionless form is

$$\frac{d\psi}{d\tau} = 1 - k\cos 2\pi\psi. \tag{11}$$

3. Analysis

3.1. Linear Stability

We solve for the phase relation that is approached during synchrony, ψ^*, where ψ^* is the constant solution of $\dot{\psi} = 0$. Thus

$$\begin{aligned} 0 &= 1 - k\cos 2\pi\psi^* \\ \cos 2\pi\psi^* &= \frac{1}{k} \\ 2\pi\psi^* &= \pm\cos^{-1}\frac{1}{k} \\ \psi^* &= \pm\frac{1}{2\pi}\cos^{-1}\frac{1}{k}. \end{aligned} \tag{12}$$

To find which of the solutions is stable, we'll evaluate $\frac{d\dot{\psi}}{d\psi}$ at each solution

$$\frac{d\dot{\psi}}{d\psi}(\psi^*) = 2k\pi\sin\left(2\pi\psi^*\right) \tag{13}$$

$$= 2k\pi\sin\left(\pm\cos^{-1}\frac{1}{k}\right). \tag{14}$$

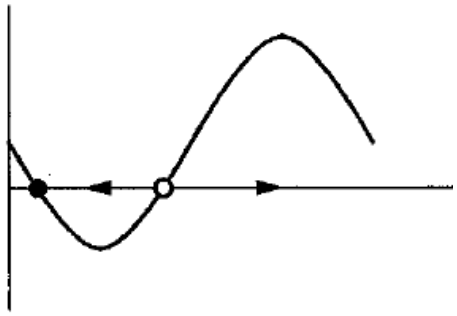

Figure 2: *Phase line for (11) with $k > 1$. When $k = 1$, a bifurcation occurs and a single fixed point emerges. When $k < 1$ there fails to be any fixed points and external desynchronization occurs.*

Because the sine function is positive over all the values for which inverse cosine is defined (namely [0,π]), the stable solution is

$$\psi^* = -\frac{1}{2\pi}\cos^{-1}\left(\frac{1}{k}\right). \tag{15}$$

3.2. Further Analysis

One drawback of the PHASE model is that it incorrectly predicts that sleep rarely occurs outside of a 10-hour window centered around temperature troughs, whereas in free-run subjects, sleep also occurred frequently at about 9 hours after the temperature trough. In other words, the data shows that the probabilty of falling asleep significantly increases at two distinct phases, making it a bimodal distribution. So, an effective remedy of this issue must change the unimodal distribution of sleep onset predicted by the PHASE model to a bimodal distribution. We will attempt to do this by introducing a correction term to the sleep-wake oscillator. Our new system looks like

$$\dot{\theta}_1 = \omega_1 - C_1 \cos 2\pi(\theta_2 - \theta_1) \tag{16a}$$

$$\dot{\theta}_2 = \omega_2 + C_2 \cos 2\pi(\theta_1 - \theta_2) + C_3 e^{-\left(\frac{\sin^2 \pi(\theta_1 - \mu_1)}{\sigma_1} + \frac{\sin^2 \pi(\theta_2 - \mu_2)}{\sigma_2}\right)}. \tag{16b}$$

We first notice that we have an expression that is reminiscent of a normal distribution. Although they are not normal distributions (because they are not scaled), they function much like a normal distribution would. These will function as our "on-off switch" for the correction term. If θ_1 and θ_2 simultaneously fall

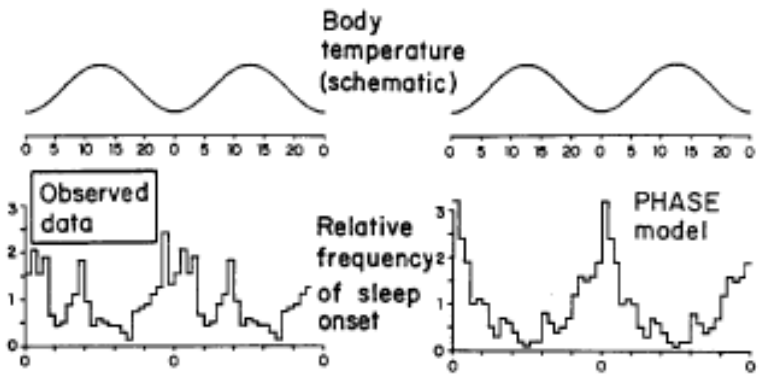

Figure 3: *As seen in the frequency diagrams below, there is a discrepancy between the PHASE model and pooled data. The PHASE model predicts a unimodal distribution with sleep mostly occuring near temperatire troughs. The data shows another peak at about 9 hours after the peak, making it bimodal.*

within a certain range (determined by σ_1 and σ_2) of their respective "means" μ_1 and μ_2, the sleep cycle will be accelerated, effectively inducing sleep. While θ_1 and θ_2 do not simultaneously fall within their ranges, the entire correction term is essentially zero and will have negligible affect on the overall system. What this allows us to do is to take sleep onsets for which the original PHASE model *incorrectly* predicts happen at a a certain temperature phase and move them to a temperature phase that is more reflective of the data. By choosing σ_1 and σ_2 (which loosely function as our "standard deviations") to be sufficiently small, we can ensure that the correction term is only activated when it hits a certain temperature-sleep phase ratio.

4. Results

Looking back at our original model, let's see what it has to say about the relationship between the circadian phase ϕ_s and sleep duration ρ. Experimental data shows that sleep beginning near temperature peaks tend to be longer than those that begin near temperature troughs. To make analysis possible, we will make the simplifying assumption that the sleep phase sends essentially no feedback into the circadian temperature phase (which is not unreasonable, given the data). The

circadian oscillator now moves at a constant rate. Scaling to that rate, equation (1a) becomes

$$\dot{\theta_1} = 1 \tag{17}$$

and by arbitrarily setting $\theta_1(0) = 0$,

$$\theta_1(t) = t. \tag{18}$$

Solving for $\theta_2(t)$ is a bit more difficult. Our game plan will be to figure out $\psi(t)$ and use that to determine $\theta_2(t) = \theta_1(t) - \psi(t)$. We know that

$$\dot{\psi} = \Omega - C\cos 2\pi\psi \tag{19}$$

where Ω, in this case, is $1 - \omega_2$. As before, letting $\tau = \Omega t$,

$$\psi' = 1 - k\cos 2\pi\psi. \tag{20}$$

Separate variables and integrate to get

$$\int \frac{d\psi}{1 - k\cos 2\pi\psi} = \int d\tau. \tag{21}$$

Substitute $u = \tan \pi\psi$. Then $\cos 2\pi\psi = \frac{1-u^2}{u^2+1}$. Substitute these into (20) to get

$$\frac{1}{2\pi}\int \frac{\frac{2du}{u^2+1}}{1 - k\left(\frac{1-u^2}{u^2+1}\right)} = \int d\tau. \tag{22}$$

Simplify and factor $(1-k)$ from integral to get

$$\frac{1}{\pi(1-k)}\int \frac{du}{u^2\frac{(1+k)}{(1-k)} + 1} = \int d\tau \tag{23}$$

Let $z^2 = \frac{u^2(1+k)}{(1-k)}$. Then

$$\frac{\sqrt{1-k}}{\pi(1-k)\sqrt{1+k}}\int \frac{dz}{z^2+1} = \tau + \text{constant}. \tag{24}$$

Since the antiderivative of (24) is $\tan^{-1} z$, we can back substitute to get

$$\frac{1}{\pi\sqrt{1-k}\,\sqrt{1+k}}\tan^{-1}\left(\frac{\tan(\pi\psi)\sqrt{1+k}}{\sqrt{1-k}}\right) = \Omega t + \text{constant}. \tag{25}$$

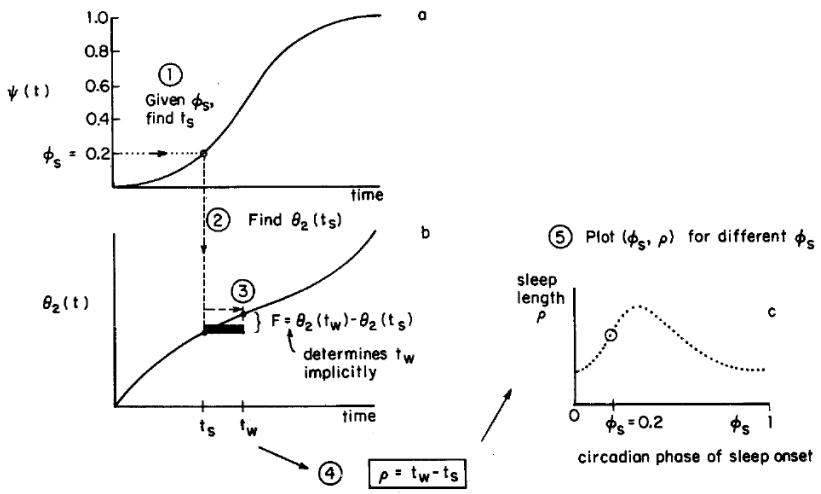

Figure 4: *1) Pick a temperature phase at sleep onset and find the time at which it happens. 2) Find the sleep phase at that time. 3) Add F to the sleep phase to find the wake time. 4) Subtract the time at wake from the time at sleep to get the sleep length. 5) Make a graph of all possible values*

Writing ψ explicitly as a function of t yields

$$\psi(t) = \frac{\tan^{-1}\left(b\tan\left(\pi\beta t + C_0\right)\right)}{\pi}, \tag{26}$$

where

$$b = \sqrt{\frac{1-k}{1+k}} \quad \text{and} \quad \beta = \Omega\sqrt{1-k^2}$$

and C_0 is a constant that contains our initial condition, ψ_0, and parameter values Ω and C. With (26), we now have a way of determining $\theta_2(t)$, which is $t - \psi(t)$. We will use graphical methods to determine the ρ to ϕ_s relationship by following the steps in Figure 4.

5. Discussion

We have reviewed a relatively simple model of sleep behavior in free-run subjects. This model is simple enough for us to retrieve useful data from it using analytic and graphic methods. We are able to establish synchrony and de-synchrony by varying parameters and rewrite it in dimensionless form with only one parameter. We have also looked at a corrected version of the PHASE model. A huge downside to this correction is that the model is no longer tractable, which was the primary

motivation for the PHASE model in the first place. The correction is also in no way informed by any biological or psychological processes endogenous of the human body; it is merely a cooked up way of getting the data to match a little bit better. Further work with the corrected model would include optimizing the parameters to get an optimal shift of sleep onsets.

References

[1] Czeisler, C. A. (1978). Human circadian physiology: Internal organization of temperature, sleep-wake and neuroendocrine rhythms monitored in an environment free of time-cues. Ph.D. thesis, Stanford University, Stanford, CA.

[2] Siffre, M. (1975). Six months alone in a cave, *National Geographic*, 147(3), 426-435.

[3] Strogatz, S. (1987). Human sleep and circadian rhythms: a simple model based on two coupled oscillators, *J. Math. Biol*, 25: 327-347.

[4] Wever, R. (1979). *The circadian system of man*. New York: Springer.

[5] Holzman, D. (2010) Environmental health perspectives-What's in a color? The unique human health effects of blue light, *Environ Health Perspect*, 118(1), A22-A27.

Chaos in a Model of Duopoly Pricing

Joseph Kincanon
Gonzaga University
Department of Economics
jkincanon@zagmail.gonzaga.edu

Matthew Krick
Gonzaga University
Department of Mathematics
mkrick@zagmail.gonzaga.edu

Abstract

The French mathematician Augustin Cournot introduced a theory of competition in 1838 to study a market structure, known as a duopoly, in which two firms compete in the absence of other competitors on the amount of product output [2]. We report on the work of Puu [4], in which he examines Cournout's duopoly theory under the simplifying assumptions of constant unit production costs and isoelastic demand. Puu examines two cases: (i) each firm adjusts its output in the current time-period based upon its competitor's production in the previous time-period, and (ii) each firm adjusts their production in the current time-period based on a weighted average of its previous production and that of its competitor. By examining the reaction functions of the firms, it is found that as a model parameter is varied, the stable fixed point known as the Nash Equilibrium becomes unstable and a period doubling route to chaos occurs. We also consider an extension of Puu's work by introducing a third competitor to form a triopoly. Although Puu's assumptions make the model unrealistic for serious economic forecasting, the inherent chaotic behavior is interesting to study from a mathematical context.

1. Introduction

T. Puu [4] investigates the Cournot duopoly model. Under the assumptions of isoelastic demand and constant unit production costs, the duopolistic Cournot model exhibits chaotic behavior when the parameter values are within a certain interval.

A duopoly is a market in which only two firms provide a certain product or service or there are only two firms that have market power; that is, there are two firms with the ability to raise and maintain prices above the level that would be

expected in the presence of competition. A third firm could exist in a duopoly, but if they do not impact price of the market good, then they are essentially irrelevant and the market is a duopoly.

We examine the Cournot model for duopolies [2], which employs the following basic assumptions: firms are competitive, that is, they do not collude, and the quantity of goods produced by the individual firms depend on the quantity produced by the competing firm. This is due to the assumption that firms adjust prices of their goods by adjusting the quantity they produce, and that price is based on the total quantity of goods produced in the market. As total quantity produced rises, price will decrease, and as total quantity produced falls, prices will rise. The implications of this dynamic are that it is in the best interest of both firms to not produce too many units of the good, otherwise the price level will not be high enough for them to cover their costs of production. If the firms choose to operate at a relatively low level of production, then the competing firm will increase their quantity. By doing this, the high quantity firm benefits from a high price due to their competitor producing few units of the good, and they also sell more units of the good.

To assist with understanding the paper, let us review some economic terminology and concepts. A demand curve is a curve that shows the relationship between the price and the quantity demanded of a good, with the variables having a negative correlation. As price of a good increases, the quantity demanded for the good decreases. This relationship also holds in reverse, with quantity demanded for a good rising when the price of the good drops.

Elasticity describes how sensitive quantity demanded is to price change. A highly elastic demand curve would mean that a small increase in price would lead to a large decrease in quantity demanded, and a small decrease in price would lead to a large increase in quantity demanded. An isoelastic demand curve is a demand curve in which the elasticity is constant for every given point along the curve.The general isoelastic demand function is given by

$$Q(p) = Ap^{\eta}$$

where A and η are constants. The parameter η represents the constant elasticity of demand. This assumption is used in the definition of price given by Equation (1) of the next section. On a non-isoelastic demand curve, the price sensitivity of a good would change depending on the current quantity demanded and the current price.

A firm that has constant unit production costs (also known as constant marginal costs) is a firm in which producing in bulk does not decrease the cost of producing each unit of good (no economies of scale). For example, if a soda company were to have constant unit production costs, this would mean that the cost per bottle

would not change if they produced ten bottles of soda, or one-million bottles of soda.

Finally, the Cournot Nash Equilibrium is the quantity of goods produced by the firms in a duopoly in which they would make less profit if they increased or decreased their chosen quantities [3]. To better illustrate this, let us assume that two firms in a duopoly are currently producing at their Nash Equilibrium quantities. If either firm were to try to increase their quantity production levels, the negative impact from the drop in the price on their profits would outweigh the profit increase from selling more units of their good. If either firm were to decrease their quantity production levels, the positive effect on the firms' profits from the increase in price would be outweighed by the negative impact the lower level of sales would have on their profits. The Cournot Nash Equilibrium is the more specific version of the general Nash Equilibrium that focuses on the quantitiy the firms produce due to the nature of the Cournot model.

2. Derivation of the Mathematical Models

Below we define the variable of the Cournot model. We note that the variables are dimensionless.

$p =$ price
$x =$ supply of first competitor
$y =$ supply of second competitor
$a =$ constant unit cost of first firm
$b =$ constant unit cost of second firm

We will begin by defining price as

$$p = \frac{1}{x+y}. \tag{1}$$

The denominator is simply the sum of the quantity of goods supplied by the two firms.

We can now represent profit for each firm as the difference of revenue (the product of quantity and price) and cost (the product of unit production cost and quantity). We will define Π_1 as profit for firm 1, and Π_2 as profit for firm 2.

$$\Pi_1(x,y) = \frac{x}{x+y} - ax \tag{2a}$$

$$\Pi_2(x,y) = \frac{y}{x+y} - by \tag{2b}$$

To find where the firms maximize profit, first we will take the partial of Π_1 with respect to x and the partial Π_2 with respect to y. It is sufficient to take the partial of Π_1 with respect to x and of Π_2 with respect to y since x corresponds only to the quantity produced by firm 1, and y corresponds only to the quantity produced by firm 2.

$$\frac{\partial}{\partial x}\left(\frac{x}{x+y} - ax\right) = \frac{(x+y)-x}{(x+y)^2} - a \tag{3a}$$

$$\frac{\partial}{\partial y}\left(\frac{y}{x+y} - by\right) = \frac{(x+y)-y}{(x+y)^2} - b \tag{3b}$$

We now set the partial derivatives in Equation (3) equal to zero to obtain

$$\frac{y}{(x+y)^2} - a = 0,$$
$$\frac{x}{(x+y)^2} - b = 0.$$

Solving for x in terms of y for the former, and solving for y in terms of x for the latter, we produce the reaction functions

$$x(y) = \sqrt{\frac{y}{a}} - y \tag{5a}$$

$$y(x) = \sqrt{\frac{x}{b}} - x. \tag{5b}$$

The focus of the Cournot Model are these reaction functions. The reaction functions show that x depends on a and y, and y depends on b and x. The goal of a typical firm is to maximize profits. We are able to find profit maximizing functions for the two firms in this model by substituting the reaction functions into the profit functions, as follows

$$\frac{\sqrt{\frac{y}{a}} - y}{\left(\sqrt{\frac{y}{a}} - y\right) + y} - a\left(\sqrt{\frac{y}{a}} - y\right) = 1 - 2a\sqrt{\frac{y}{a}} + ay,$$

$$\frac{\sqrt{\frac{x}{b}} - x}{\left(\sqrt{\frac{x}{b}} - x\right) + x} - b\left(\sqrt{\frac{x}{b}} - x\right) = 1 - 2b\sqrt{\frac{x}{b}} + by.$$

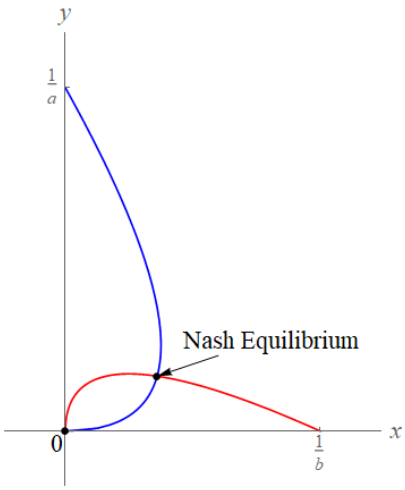

Figure 1: *Reaction Functions of Equations (5). The blue curve is a plot of $x(y)$ and the red curve is a plot of $y(x)$. The intersection of the two curves represents the Nash Equilibrium Point.*

Using the above, we define our maximized profit functions by

$$\Pi_{m1} = 1 - 2\sqrt{ay} + ay, \tag{7a}$$

$$\Pi_{m2} = 1 - 2\sqrt{bx} + bx. \tag{7b}$$

An important note to make is that the maxima are attained at $y = \frac{1}{4b} = x$ and $x = \frac{1}{4a} = y$. This will be important later.

Figure 1 shows both reaction functions on the x, y plane. Firm 1's reaction function touches the y-axis at $(0, \frac{1}{a})$ and Firm 2's reaction function touches the x-axis at $(\frac{1}{b}, 0)$. The significance of these points will be discussed later. This system has two fixed points, the origin $(0, 0)$ and the intersection point of the reaction functions, which is the Nash Equilibrium point. The intersection point is found by solving simultaneously for the two reaction functions, which results in the following

$$(x^*, y^*) = \left(\frac{b}{(a+b)^2}, \quad \frac{a}{(a+b)^2} \right)$$

2.1. Taking Turns Model

The first discrete time model is looking at the reaction functions when the firms adjust by taking turns. This means that firm 1 reacts or adjusts at any given time t by taking into consideration what firm 2 did at time $t-1$, and similarly, firm 2

reacts or adjusts at any given time t by taking into consideration what firm 1 did at time $t-1$.

$$x_t = \sqrt{\frac{y_{t-1}}{a}} - y_{t-1} \tag{8a}$$

$$y_t = \sqrt{\frac{x_{t-1}}{b}} - x_{t-1} \tag{8b}$$

2.2. Simultaneous Decision Model

The second discrete time model will assume that the competing firms make their decisions simultaneously. However, the firms will adjust their decisions by adjusting their previous decision toward their new optimal output. The Simultaneous Decision Model presented by Puu [4] is

$$x_t = x_{t-1} + \theta\left(\sqrt{\frac{y_{t-1}}{a}} - y_{t-1} - x_{t-1}\right), \tag{9a}$$

$$y_t = y_{t-1} + \theta\left(\sqrt{\frac{x_{t-1}}{b}} - x_{t-1} - y_{t-1}\right). \tag{9b}$$

The parameter θ lies in the interval $0 \leq \theta \leq 1$. It shows how much the firms care about the decisions of their competitor. If they do not care at all, $\theta = 0$. In this case

$$x_t = x_{t-1} \quad \text{and} \quad y_t = y_{t-1},$$

that is, their decision in the current time period is base strictly upon what they did in the previous time period. At the opposite extreme, if $\theta = 1$, we obtain the reaction functions of the Taking Turns model given by Equations (8), in which case their decision is based strictly upon the output of their competitor.

3. Linear Analysis

In this section we discuss the fixed points of the two discrete time models given by Equations (5) and (10) and their linear stability.

3.1. Taking Turns Model[1]

We begin by defining the nonlinear map $F : \mathbb{R}^2 \to \mathbb{R}^2$ by

$$F\begin{pmatrix} x_t \\ y_t \end{pmatrix} \equiv \begin{pmatrix} \sqrt{\frac{y_t}{a}} - y_t \\ \sqrt{\frac{x_t}{b}} - x_t. \end{pmatrix}$$

so that

$$\begin{pmatrix} x_{t+1} \\ y_{t+1} \end{pmatrix} = F\begin{pmatrix} x_t \\ y_t \end{pmatrix}.$$

As with one-dimensional systems, fixed points of F satisfy

$$F\begin{pmatrix} x^* \\ y^* \end{pmatrix} = \begin{pmatrix} x^* \\ y^* \end{pmatrix}.$$

It is readily seen that

$$F\begin{pmatrix} 0 \\ 0 \end{pmatrix} = \begin{pmatrix} 0 \\ 0 \end{pmatrix},$$

thus the origin is a fixed point. A second nontrivial fixed point is found to be

$$\begin{pmatrix} x_e \\ y_e \end{pmatrix} = \begin{pmatrix} \frac{b}{(a+b)^2} \\ \frac{a}{(a+b)^2} \end{pmatrix}.$$

The point $(x_e, y_e)^T$ is commonly referred to as the Nash Equilibrium of the system. Using standard techniques, we find that the Jacobian matrix of the map F is

$$J = \begin{pmatrix} 0 & \frac{1}{2}\sqrt{\frac{1}{ay}} - 1 \\ \frac{1}{2}\sqrt{\frac{1}{bx}} - 1 & 0 \end{pmatrix}.$$

Stability of the Origin. Note that the origin is a repeller (unstable) since the Jacobian matrix is unbounded as $(x, y)^T \downarrow (0, 0)^T$. Let us consider an intuitive explanation for this observation. At the point $(0, 0)^T$ neither firm is producing any product. This means that there is a market of people who want a certain good but nobody is supplying it. Eventually, one of the firms will realize that there is a market for a product or service but no product or service is in production. This will prompt the firm to enter the market. Recognizing that there is profitable business at hand, the other firm will enter the market to compete. Hence, we see that the fixed point is fundamentally unstable.

[1]This section contains substantial revisions by the editor.

Stability of the Nash Equilibrium Point. Evaluating the Jacobian matrix at the Nash Equilibrium point yields

$$J|_{(x_e,y_e)} \equiv J_e = \begin{pmatrix} 0 & \frac{-a+b}{2a} \\ \frac{a-b}{2b} & 0 \end{pmatrix}.$$

Observe that the trace of J_e equals 0 and the determinant of J_e is

$$\det(J_e) = \frac{(a-b)^2}{4ab}.$$

Thus, the characteristic polynomial is

$$\sigma^2 + \frac{(a-b)^2}{4ab} = 0,$$

which implies that the eigenvalues are pure imaginary numbers given by

$$\sigma_\pm = \pm i \frac{|a-b|}{2\sqrt{ab}},$$

where $i = \sqrt{-1}$. The condition for stability requires that $|\sigma_\pm| < 1$. Therefore, a and b must satisfy

$$(a-b)^2 < 4ab.$$

This yields

$$a^2 - 2ab + b^2 < 4ab \Rightarrow \left(\frac{a}{b}\right)^2 - 6\left(\frac{a}{b}\right) + 1 < 0.$$

Solving yields $3 - 2\sqrt{2} < a/b < 3 + 2\sqrt{2}$. This means that if the ratio of the firms' unit productions costs lies within this range, then the Nash Equilibrium fixed point is stable, if it does not, then the equilibrium point is unstable.

We now determine conditions such that $x_t, y_t > 0$ for all t, which is necessary so as to avoid complex values. It was found from Equation (8a), that the reaction functions reach their respective maxima at $y = \frac{1}{4a} = x$. In order to avoid complex numbers, we require $y(\frac{1}{4a}) < \frac{1}{a}$, that is

$$\sqrt{\frac{1}{4ab}} - \frac{1}{4a} < \frac{1}{a} \Rightarrow \frac{a}{b} < \frac{25}{4} \Rightarrow \frac{b}{a} < \frac{4}{25}$$

Similarly, using Equation (8b) we find

$$\sqrt{\frac{1}{4ab}} - \frac{1}{4b} < \frac{1}{b} \Rightarrow \frac{b}{a} < \frac{25}{4} \Rightarrow \frac{a}{b} > \frac{4}{25}$$

We see that the ratio of unit production costs must be in the interval $(\frac{4}{25}, \frac{25}{4})$ for the output of the model to be real-valued.

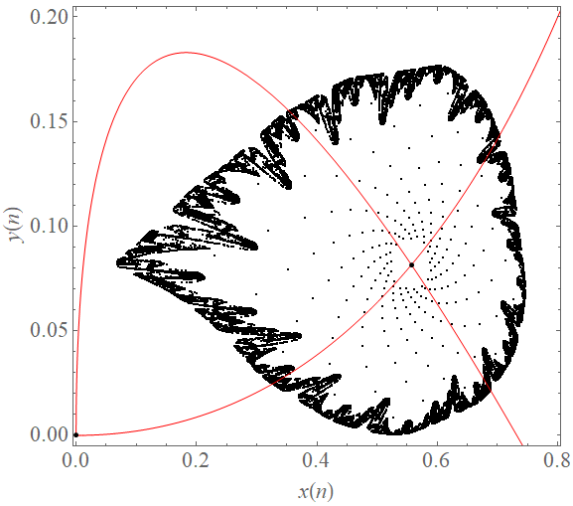

Figure 2: *Strange attractor for the Simultaneous Decision Model. The abscissa, $x(n) \equiv x_t$, represents the production level of firm 1 while the ordinate, $y(n) \equiv y_t$, represents the production level of firm 2. Starting at the initial point $(x_0, y_0) = (0.55,\ 0.07)$, Equations (9) were iterated 200,000 times using Mathematica 11.2 with $\theta = .9$, $a = .2$, and $b = 1.36592$. For these parameter values, the Nash Equilibrium point is a repeller (see Editor's note in Section 3.2) and the orbit of $(0.55,\ 0.07)$ spirals away from the unstable Nash Equilibrium to the stable "chaotic leaf".*

3.2. Simultaneous Decision Model

The fixed points and their related stability are the same for the Simultaneous Decision model as for the Taking Turns model.

Editor's note. While the Simultaneous Decision model and the Taking Turns model share the same fixed points, the economically relevant parameter values and the stability criteria for the Nash Equilibrum now depend upon the parameter θ as well as a and b. For stability, the parameters a, b and θ must satisfy

$$\theta < \frac{8ab}{(a+b)^2}. \tag{10}$$

4. Results

It is claimed that both models can exhibit chaotic behavior and an interesting chaotic attractor is produced by the Simultaneous Decision modelwhen $\theta = 0.9$ as shown in [4]. Also shown in [4] are cobweb diagrams for both models; however, we were not able to reproduce these figures.

Editor's note. Figure 2 (contributed by the editor) shows a stable chaotic attractor for the Simultaneous Decision model when $a = 0.2,\ b = 1.36592$, and $\theta = 0.9$. For these values the Nash Equilibrium is a repeller (unstable) which can be seen from Equation (10) by noting that $\theta = 0.9$ is not less than $8ab/(a+b)^2 \approx 0.8913$. Related ideas to explore are the fractal dimension of the attractor and the parameter ranges for which at least one Liapunov exponent is greater than zero.

5. Further Analysis

Puu [4] collaborated with Agliari and Gardini to examine a triopoly Cournot game with his assumptions of constant unit production costs and isoelastic demand [1]. A triopoly is just a duopoly but with three firms instead of two. We will keep all of the same variables from our duopoly model, but we will introduce some new variables. We let z be the quantity produced by firm 3, and c be the constant unit production costs of firm 3. The new price function would be

$$p = \frac{1}{x+y+z}. \tag{11}$$

The profits of the individual firms are

$$\Pi_1 = \frac{x}{x+y+z} - ax$$

$$\Pi_2 = \frac{y}{x+y+z} - by$$

$$\Pi_3 = \frac{z}{x+y+z} - cz$$

with Π_3 being the profit of firm 3, Π_2 being the profit of firm 2, and Π_1 being the profit of firm 1.

To obtain the reaction functions for the triopoly, we will take the partial

derivatives as shown

$$\frac{\partial}{\partial x}\left(\frac{x}{x+y+z}-ax\right)=\frac{(x+y+z)-x}{(x+y+z)^2}-a$$

$$\frac{\partial}{\partial y}\left(\frac{y}{x+y+z}-by\right)=\frac{(x+y+z)-y}{(x+y+z)^2}-b$$

$$\frac{\partial}{\partial z}\left(\frac{z}{x+y+z}-cz\right)=\frac{(x+y+z)-z}{(x+y+z)^2}-c$$

and then set these partial derivatives equal to 0

$$x(y,z)=\sqrt{\frac{y+z}{a}}-y-z$$

$$y(x,z)=\sqrt{\frac{x+z}{b}}-x-z$$

$$z(x,y)=\sqrt{\frac{x+y}{c}}-x-y.$$

Looking at the reaction functions for the triopoly, we can see that they are very similar to the duopoly reaction functions. However, let us perform an experiment to show an interesting phenomenon that occurs in the Cournot triopoly.

5.1. Triopoly Experiment

To see the interesting behavior of the triopoly model, we will compare the results of quantity of goods produced by the individual firms in both the duopoly and triopoly model.

First we will assign arbitrary constant unit production costs to the firms, with $a = 0.2$, $b = 0.3$, and $c = 0.4$. Using these parameter values for the duopoly reaction functions and solving for x and y, we get $x = 1.2$ and $y = 0.8$ (c is irreverent for the duopoly model). When these values are applied to the triopoly reaction functions, we obtain $x \approx 1.23$, $y \approx 0.74$, and $z \approx .25$. When the third firm enters the market, intuition tell us that due to increased competition, firms already in the market will lose market share (customers) which should be seen

as lower quantities produced by the individual firms. Despite this being true for firm 2 with the value of y being lower with firm 3 entering the market, firm 1 actually increases their quantity produced with firm 3 entering into the market. A possibility for this occurring could be that firm 3 entering the market impacts the profit of firm 2 more severely than the profit of firm 1 due to firm 1 having relatively low unit production costs. Looking at equation (11), we notice that the price decreases as total quantity produced rises. When firm 3 entered the market, the price of the good lowered, which then causes revenue for all three firms to drop. However, due to firm 2 having higher unit production costs than firm 1, firm 2 would have to decrease output to increase the price so that firm 2 can cover their costs of production. When this occurs, firm 1 would increase quantity produced and would still make a profit with a low-priced good, due to their low unit production costs.

6. Discussion

We see that the simple Cournot Duopoly model, given Puu's conditions of isoelastic demand and constant unit production costs produces chaotic behavior within certain parameter values. Due to the minimal number of parameters and strict conditions associated in the model, it does not necessarily model a realistic duopoly competition scenario. With this in mind, we must take into consideration that this model is mostly useful from a mathematical analysis standpoint, and for qualitative analysis of economic situations. The model is intriguing largely due to the fact that we can observe chaotic behavior within such a simple model, and demonstrates that minor adjustments in initial conditions can cause period doubling routes to chaos. In order to better represent this model as economically feasible, we would relax the conditions of constant unit production cost, and possibly of isoelastic demand as well. This would make the model more realistic but also more difficult to analyze mathematically.

Acknowledgments

We would like to thank Dr. Richard Cangelosi for his guidance on this project, especially with understanding the chaotic features of the model.

Author Contribution

Joseph Kincanon analyzed the economic implications of the model, created the idea and performed the further analysis of the triopoly model, and performed the

linear stability analysis of the $(0,0)$ fixed point. Matthew Krick reproduced the mathematics in the paper, *Chaos in Duopoly Pricing* by T. Puu [4], and performed the linear stability analysis for the Nash Equilibrium fixed point. The rest of the article was worked on cooperatively.

References

[1] Agliari, Anna, et al. The Dynamics of a Triopoly Cournot Game. *Chaos, Solitons and Fractals*, vol. 11, no. 15, 2000, pp. 2531-2560., doi:10.1016/s0960-0779(99)00160-5.

[2] Cournot, Augustin. *Researches into the Mathematical Principles of the Theory of Wealth*. The MacMillan Company, 1838, https://www3.nd.edu/ tgresik/IO/Cournot.pdf

[3] Nash, J. F. Equilibrium Points in n-Person Games. *Proceedings of the National Academy of Sciences*, vol. 36, no. 1, Jan. 1950, pp. 48-49., doi:10.1073/pnas.36.1.48.

[4] Puu, T. Chaos in Duopoly Pricing. *Chaos, Solitons and Fractals*, vol. 1, no. 6, 1991, pp. 573-581., doi:10.1016/0960-0779(91)90045-b.

Analysis of a Proposed Genetic Toggle Switch

Elijah Michaelson

Gonzaga University
Department of Computer Science
emichaelson@zagmail.gonzaga.edu

Abstract

The composition of simple genetic regulatory elements facilitates the control of gene expression levels in biological systems. The study of these mechanisms yields crucial insight into the implementation details of cell-fate decision processes. Here we present an analysis of a two dimensional, highly nonlinear model of a proposed genetic toggle switch presented in [1]. This analysis includes quantitative applications of linear stability analysis and bifurcation analysis to elucidate the critical properties of the system. A qualitative explanation of the underlying factors that determine these critical properties is included as well. We find that the model yields the desired properties of a genetic toggle switch, notably bistability characterized by a separatrix isolating two basins of attractions containing the high and low states of the switch. Only if a number of requirements are met does this model manifest these properties.

1. Introduction

In biological systems, genetic regulatory circuits control the expression of genes through the use of various molecular regulators. Notable among the collection of regulatory elements that interact to determine gene expression levels are repressors, promoters, and inducers. From these simple elements it has been shown [1] that it is possible to construct a mechanism in gene-regulatory networks that acts as a genetic toggle switch. The existence of this mechanism results in two steady states within the system.

We investigate the mathematical nature of this mechanism by examining the two-dimensional, nonlinear model that governs its behavior. Additionally, we

investigate the conditions necessary for this bistability and the properties of the resulting system under various constraints. We give a qualitative description of the proposed model and apply linear stability analysis and bifurcation analysis to the system to elucidate these properties. This research contributes to the theoretical understanding of how a simple mechanism, such as the genetic toggle switch, can be implemented in biological systems and the properties that arise from the existence of such mechanisms. The understanding of these regulatory switches has implications for understanding the components in the cell-fate decision making process, and sheds light on a given initial condition's effect of the eventual expression of some gene. We promote this line of inquiry by studying the qualitative behavior a collection of these simple mechanisms can yield in regulatory circuits.

2. Mathematical Model

The dimensionless mathematical model describing the behavior of the genetic toggle was derived in [1] from a biochemical rate equation formulation of gene expression from [2-5]. It is given as

$$\frac{du}{dt} = \left(\frac{\alpha_1}{1+v^\beta}\right) - u \tag{1}$$

$$\frac{dv}{dt} = \left(\frac{\alpha_2}{1+u^\gamma}\right) - v \tag{2}$$

In this model u is the concentration of repressor 1, v is the concentration of repressor 2, α_1 is the effective rate of synthesis of repressor 1, α_2 is the effective rate of synthesis of repressor 2, β is the cooperativity of repression of promoter 2 and γ is the cooperativity of repression of promoter 1 [1].

Cooperative repression of constitutively transcribed promoters, a fundamental aspect of the genetic toggle switch, is manifested in the first term in each equation. Degradation/dilution of the repressors, another fundamental aspect of the genetic toggle switch, is manifested in the second term in each equation. α_1 and α_1 describe the net effect of RNA polymerase binding, open-complex formation, transcript elongation, transcript termination, repressor binding, ribosome binding and polypeptide elongation [1].

The bistability of the model, which gives rise to the desired properties of the genetic toggle switch, are the result of the single unstable and two stable fixed points from the intersection of the nullclines

$$\frac{du}{dt} = 0, \quad \frac{dv}{dt} = 0. \tag{3}$$

Figure 1: $\beta, \gamma = 0$

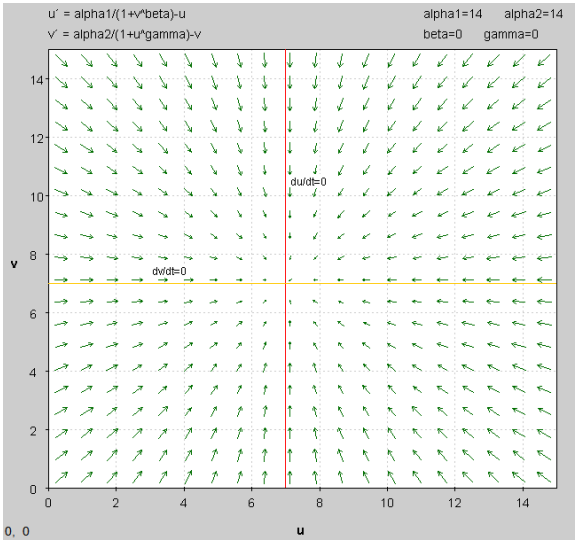

3. Results

Linearization of the model yields the Jacobian J such that

$$J = \begin{bmatrix} -1 & \frac{-\alpha_1 \beta v^{\beta-1}}{(1+v^\beta)^2} \\ \frac{-\alpha_2 \gamma u^{\gamma-1}}{(1+u^\gamma)^2} & -1 \end{bmatrix}, \tag{4}$$

with

$$tr(J) = (-1) + (-1) = -2 \tag{5}$$

$$det(J) = (-1)(-1) - (\frac{-\alpha_1 \beta v^{\beta-1}}{(1+v^\beta)^2})(\frac{-\alpha_2 \gamma u^{\gamma-1}}{(1+u^\gamma)^2}) \tag{6}$$

The cooperativity of repression of the promoters, quantified by parameters β and γ in (1) and (2), determine the qualitative shape of the nullclines and consequently the number of fixed points existing within the system. In physical systems, this cooperativity can result from multimerization of the repressor proteins and cooperative binding of the multimers to more than one operator site in the promoter region [1]. In the extreme case of an absence of any cooperativity, described by $\beta, \gamma = 0$, the phase plane exhibits a single fixed point at $(\alpha_1/2, \alpha_2/2)$. Evaluating (4) at this point yields $tr(J) = -2 < 0$ and $det(J) = 1 > 0$, indicating that the fixed point is stable for all values of α_1 and α_2. This monostable property of the system is present for all $\beta, \gamma < 1$, although finding an analytic solution for

Figure 2: $\beta, \gamma < 1$

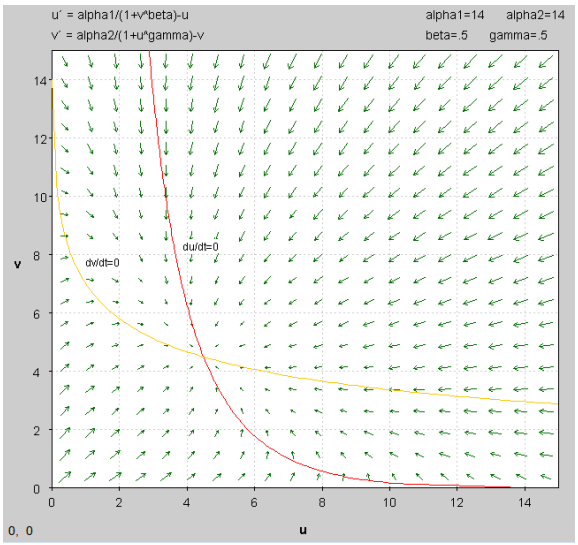

the fixed point becomes nontrivial. An example of a system with $\beta, \gamma < 1$ can be seen in Figure 2.

At $\beta, \gamma > 1$, the characteristics for the genetic toggle switch become possible. In physical terms this indicates that the existence of a genetic toggle switch requires cooperative repression of transcription. The bistability is a result of the nullclines obtaining a sigmoidal shape for $\beta, \gamma > 1$, which intersect at three points. This is illustrated in Figure 3.

Figure 3: $\beta, \gamma > 1$ *and Balanced* α_1, α_2

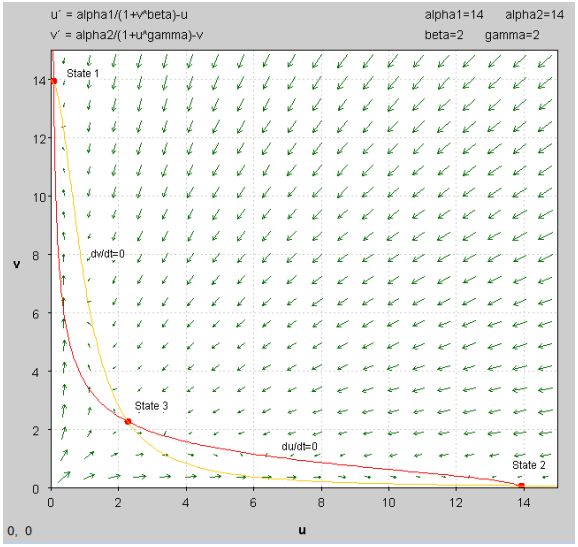

Evaluating (4) at the fixed points in Figure 3 yields:

Table 1: *Evaluating J at the 3 Fixed Points*

Fixed Point	Trace	Determinant	Classification
State 1	-2	.98	Stable
State 2	-2	.98	Stable
State 3	-2	-1.81	Saddle Point

It is possible, however, for the system to only exhibit a monostable state for $\beta, \gamma > 1$, as illustrated in Figure 4. This arises when the rate of synthesis of the two repressors are not balanced, as in Figure 4. In this case, the parameter value of α_1 is an order of magnitude greater than he parameter value of α_2. Hence, the system becomes monostable. Evaluating (4) at the only fixed point yields $tr(J) = -2 < 0$ and $det(J) = 1 > 0$, indicating that the system has a single, stable fixed point.

Figure 4: $\beta, \gamma > 1$ *and Unbalanced* α_1, α_2

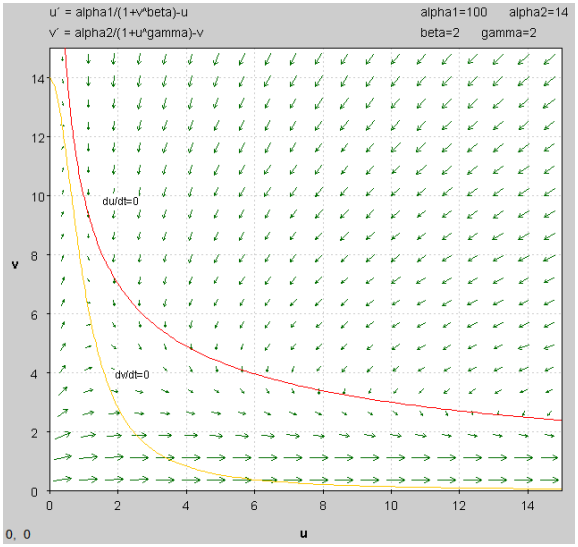

Thus, another necessary condition for the toggle switch is that parameters α_1 and α_2 must be balanced. This condition is illustrated in Figure 5 from [1].

Figure 5: *Bistable Region*

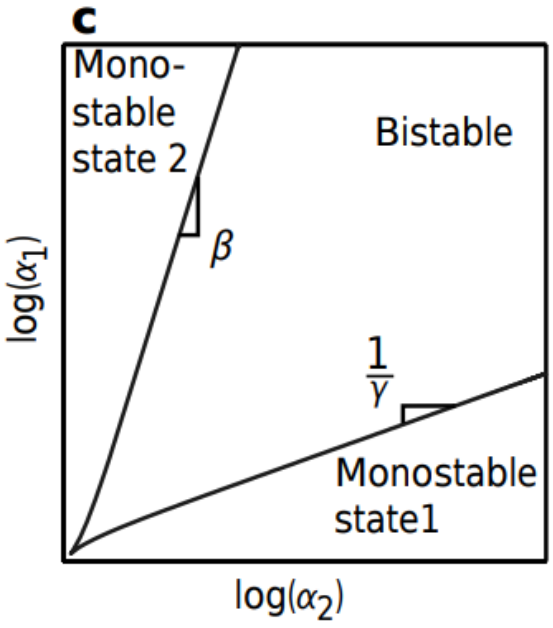

Equation (7) gives us a hint as to where the bifurcation point and the birth of bistability occurs. Specifically, there is a bifurcation at

$$1 = \left(\frac{-\alpha_1 \beta v^{\beta-1}}{(1+v^{\beta})^2}\right)\left(\frac{-\alpha_2 \gamma u^{\gamma-1}}{(1+u^{\gamma})^2}\right) \tag{7}$$

When the properties of the genetic toggle switch are satisfied, the phase space is composed of two basins of attraction separated by a separatrix. When the initial condition is anywhere above the separatrix, the system will eventually settle in State 1. When the initial condition is anywhere below the separatrix, the system will eventually settle in State 2. This is illustrated in Figures 6 and 7.

Figure 6: *Time Series for* $(u_0, v_0) = (10, 12)$

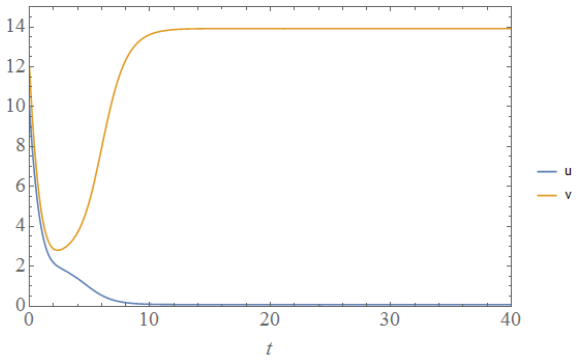

Figure 7: *Separatrix and Various Initial Conditions*

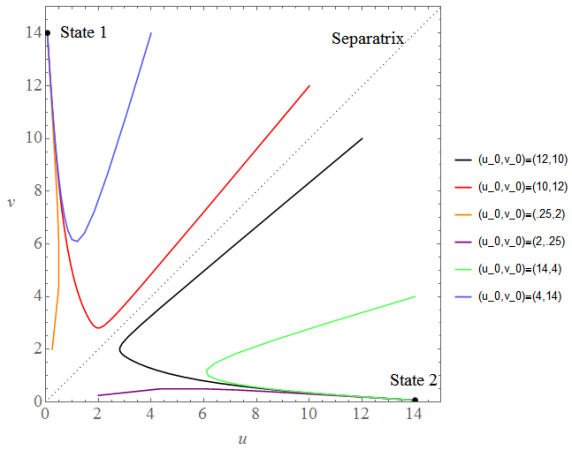

4. Discussion

In this analysis we have seen that the model does not guarantee the properties of a genetic toggle unless two conditions are satisfied.

First, the cooperativity of repression of both promoter 1 and promoter 2, quantified in parameters β and γ, must be greater than 1. This indicates that cooperative repression of transcription is a necessary property for this system's bistability. Second, the effective rate of synthesis, which is quantified in α_1 and α_2 must be balanced. If the ratio of synthesis for the individual repressors is too large, then only a monostable state results. Figure 5 and Equation (7) provide a description of this bistable region.

The key properties of the toggle switch are the separatrix, which separate the two basins of attraction, and bistability. Using a biological interpretation, these properties result in exclusive gene expression. This is a fundamental mechanism in the understanding and production of complex genetic networks.

5. Further Analysis

Extending this model to include a third repressor concentration would be an interesting next step. The work done in this analysis could be used to ensure that the resulting three-switch has the desired biological properties. Additionally, it was proposed in [1] that the toggle switch forms an addressable cellular memory unit. Understanding how these genetic switches can be used to form self-contained genetic programs would advance this work.

References

[1] Gardner, Timothy S., Charles R. Cantor, and James J. Collins (2000). Construction of a genetic toggle switch in Escherichia coli. *Nature* 403(6767), 339.

[2] Edelstein-Keshet, L. (1988). *Mathematical Models in Biology.* McGraw-Hill, New York.

[3] Kaplan, D. & Glass, L. (1995). *Understanding Nonlinear Dynamics.* Springer, New York.

[4] Yagil, E. & Yagil, G. (1971). On the relation between effector concentration and the rate of induced enzyme synthesis. *Biophys.* J. 11, 11-27.

[5] Rubinow, S. I. (1975). *Introduction to Mathematical Biology.* Wiley, New York.

A Model of Immune System Response to Tumor Growth

Lydia Pane

Gonzaga University
Department of Mathematics
lpane@zagmail.gonzaga.edu

Abstract

Nonlinear dynamical models of immune-tumor interaction give insight into which immune defenses are most effective in tumor lysis. We analyze three coupled nonlinear differential equations that incorporate CD8+ T-cells and NK cells to understand the destructive dynamics and possible immunotherapy applications. The accuracy of the T-cell competition term is analyzed through data fitting, and it is concluded that a rational form of the competition term is necessary. We then successfully reproduce the full immune system and the lack NK cell simulations of the mathematical solution, but find a discrepancy in the simulation in the absence ot T-cells. Last, we make two simplifying assumptions in which tumor cell population is significantly larger than T-cell population and vice versa. The analysis of large tumor cell population show that with no competition term of T-cells/tumor cells the model acts the same as when no T-cells are present. When the T-cell population significantly exceeds tumor cells the model shows tumor growth control for certain challenges of tumor.

1. Introduction

The Immune system has many mechanisms to deal with tumor growth, however cancer still persists as the second deadliest disease in the United States [1]. The development and understanding of the immune system response to tumor cells is crucial to creating new potential cures for cancer in the field of immunotherapy. Immunotherapy utilizes substances from other organisms to treat cancer by helping the immune response. Mathematical modeling of immune response to

tumors is extremely important to quantify new cancer treatment's effectiveness as well as advance immunotherapy techniques. Many models have been proposed for the immune response of tumors, see for example [2]. The focus of [2] is on natural Killers (NK) and CD8+ T-cells, two suppressors for various tumor cell lines.

T-cells are a type of white blood cell generated in the thymus that circulate through the body looking for abnormalities. The T-cell is the primary response of the immune system to infected cells because they have direct recognition and destruction tools. Specifically, CD8+ T-cells differentiate into cytotoxic cells that look for pathogens and kill infected cells within the body.

Natural Killer cells are also a type of lymphocyte and are part of the Innate immune system. NK cells are activated in response to interferons or Macrophage-derived cytokines. NK cells are unique in that they do not require pre-stimulation before they perform their function. These cells are activated by cytokines which trigger them to infiltrate pathogen-infected tissue. NK will cause apoptosis of the cell, not allowing for spread of the virus.

The model presented in [2] utilizes data from mouse tumor cell lines where modifications were created to express higher levels of immune bound ligands. Human data from melanoma patients treated with highly reactive T-cells was also relied on. The analysis of the model demonstrates the effectiveness of immune response from CD8+ T-cells as well as NK cells. Immunotherapy will also be explored with a further understanding of how the immune response works and what can be strengthened to try and defeat cancer. This paper aims to analyze the proposed model and interpret the implications of the model to cancer research.

The model under consideration is highly nonlinear with 16 parameters and cannot be nondimentionalizied efficiently so the authors rely on numerical analyses to explore the model's dynamics. We will show the thought process behind the competition term for CD8+ T-cell/tumor lysis and include the data fitting experiments of [2]. We then recreate computational solution graphs to the model and compare this with the solutions applying the absence of T-cells and then NK cells. We conclude the same as [2], that both NK and T-cells are needed to control tumor growth. We then explore two simplifying assumptions which allow us to employ certain standard analytic techniques. In particular, we consider the special cases where it is assumed that (i) the tumor cell population is significantly larger than the CD8+ T-cell population and (ii) the CD8+ T-cell population is significantly larger than the tumor cell population.

2. Mathematical Model

The Mathematical Model in [2] that we will be considering has been developed using the mouse and human data mentioned previously. The system utilizes the results of the mouse data to show that rejection of tumors in mice were largely due to NK and CD8+ T-cell interactions with tumor cells. The human data shows patients with melanoma who were treated with highly selective T-cells that exhibited strong immune responses. The data considered creates biological assumptions that help shape the model. They are as follows:

1. Tumor cells grow logistically in the absence of immune response.
2. Both NK and CD8+ T-cells can kill tumor cells.
3. Tumor cells have the potential to cause cytocidal activity in noncytotoxic cells.
4. NK cells are always present even in the absence of tumor cells
5. CD8+ T-cells are recruited once tumor cells are present.
6. Each NK and CD8+ T-cell will eventually become inactivated after a certain number of encounters with tumor cells.

The assumptions above lead to three coupled differential equations in which the cell populations are represented by

$T(t)$, tumor cell population at time t.
$N(t)$, total level of NK cell effectiveness at time t.
$L(t)$, total level of tumor specific CD8+ T-cell effectiveness at time t.

In terms of representations, the equations can be explained by:

rate of change of tumor cell population = (growth and death rate) - (cell-cell kill rate)

rate of change of NK or T-cells populations = (growth and death rate) + (recruitment rate) - (inactivation rate)

Substituting the proper mathematical forms for the growth and death rate, the cell-cell kill term, the recruitment rate, and the activation rate yields the following system of differential equations.

$$\frac{dT}{dt} = aT\,(1 - bT) - cNT - D \tag{1}$$

$$\frac{dN}{dt} = \sigma - fN + \frac{gT^2}{h+T^2}N - pNT \tag{2}$$

$$\frac{dL}{dt} = -mL + \frac{jD^2}{k+D^2}L - qLT + rNT \tag{3}$$

where,

$$D = \frac{d\left(\frac{L}{T}\right)^{\lambda}}{s+\left(\frac{L}{T}\right)^{\lambda}}T. \tag{4}$$

The first term of Eq. (1) reflects assumption (1) because if this was the only term it amounts to logistic tumor growth. The second term in Eq. (1) shows the rate at which tumor cells are killed by NK and therefore it reflects assumption (2). Eq. (4) appears at the end of Eq. (1) and can be thought of as the rate at which tumor cells die from CD8+ T-cells, though it will be explained in more detail below. Eq. (2) shows a constant rate of production of NK cells, assumption (4), through the first term, σ, as well as the death rate of NK cells in the second term. The third term expresses the recruitment rate of NK cells by presence of tumor cells and displays assumption (3). The fourth and last term in Eq. (2) shows the inactivation of NK cells by interaction with tumor cells which mathematically formats assumption (6). Eq. (3) has the same basic structure as Eq. (2) and uses the same assumptions, except for a few exceptions. First, there is not a constant flow of CD8+ T-cells because T-cells are only activated when tumor cells are present so this absence of a term uses assumption (5). The only other difference is that Eq. (3) has an added term at the end that accounts for the recruitment of T-cells by the interaction of NK cells and tumor cells. T-cells are recruited by the presence of tumor cells alone as well, but they activate at a higher rate when increased levels of NK cells are in the body. Figure 1 provides a description of all model parameters.

3. Results

The results of [2] rationalize the need for Eq. (4). The competition term between the tumor cells and either the NK cells or the CD8+ T-cells have fundamentally different forms. The first place to begin when creating competition terms is to make the assumption that the effector cells (NK or T-cells) reduce tumor cell population proportionally to the populations of both the effector cells and the tumor cells. This leads to simple product terms like $-cNT$ (representing the NK and tumor interaction) or $-\alpha LT$ (representing a hypothetical CD8+ T-cell and tumor interaction) in which c and α are parameters measuring the effectiveness of the immune cells. To test if these competition terms are accurate, the model was graphed against the experimental effector/target lysis data. In Figure 2, the

Parameters	Units	Estimated value	Description	Source
a	day^{-1}	5.14×10^{-1}	Tumor growth rate	(6)
b	cell^{-1}	1.02×10^{-9}	$1/b$ is tumor carrying capacity	(6)
$c(n)$	$\text{cell}^{-1}\ \text{day}^{-1}$	3.23×10^{-7}	Fractional (non)-ligand-transduced	(6)
$c(l)$		3.50×10^{-6}	tumor cell kill by NK cells	
$d(nn)$	day^{-1}	1.43	Saturation level of fractional	(6)
$d(nl)$		3.60	tumor cell kill by $CD8^+$ T cells.	
$d(ln)$		3.51	*nn*, *nl*, *ln*, *ll*: primed with	
$d(ll)$		7.17	(non)-ligand-transduced cells, challenged with (non)-ligand-transduced cells.	
$\lambda(nn)$	None	5.80×10^{-1}	Exponent of fractional tumor	(6)
$\lambda(nl)$		4.60×10^{-1}	cell kill by $CD8^+$ T cells. nn, nl, ln, ll:	
$\lambda(ln)$		9.00×10^{-1}	primed with (non)-ligand-transduced cells,	
$\lambda(ll)$		7.50×10^{-1}	challenged with (non)-ligand-transduced cells.	
$s(nn)$	None	2.73	Steepness coefficient of the Tumor-($CD8^+$ T cell)	(6)
$s(nl)$		1.61	competition term. nn, nl, ln, ll: primed with	
$s(ln)$		5.07	(non)-ligand-transduced cells, challenged	
$s(ll)$		4.00×10^{-1}	with (non)-ligand-transduced cells (smaller $s \Rightarrow$steeper curve)	
σ	cells day^{-1}	1.30×10^{4}	Constant source of NK cells.	(10)
f	day^{-1}	4.12×10^{-2}	Death rate of NK cells.	(10)
$g(n)$	day^{-1}	2.5×10^{-2}	Maximum NK cell recruitment rate by	(10, 6)
$g(l)$		$4g(n) = 2 \times 10^{-1}$	(non)-ligand-transduced tumor cells.	
h	cell^2	2.02×10^{7}	Steepness coefficient of the NK cell recruitment curve	(10)
p	$\text{cell}^{-1}\ \text{day}^{-1}$	1.0×10^{-7}	NK cell inactivation rate by tumor cells	(6)
m	day^{-1}	2.0×10^{-2}	Death rate of $CD8^+$ T cells	(27)
$j(nn)$	day^{-1}	3.75×10^{-2}	Maximum $CD8^+$ T-cell recruitment rate. nn, nl, ln, ll:	(10, 6)
$j(nl)$		3.75×10^{-2}	primed with (non)-ligand-transduced cells, challenged	
$j(ln)$		$3j(nn) = 1.13 \times 10^{-1}$	with (non)-ligand-transduced cells.	
$j(ll)$		$8j(nn) = 3.0 \times 10^{-1}$		
k	cell^2	2.02×10^{7}	Steepness coefficient of the $CD8^+$ T-cell recruitment curve	(10, 6)
q	$\text{cell}^{-1}\ \text{day}^{-1}$	3.42×10^{-10}	$CD8^+$ T-cell inactivation rate by tumor cells	(10)
r	$\text{cell}^{-1}\ \text{day}^{-1}$	1.1×10^{-7}	Rate at which tumor-specific $CD8^+$ T cells are stimulated to be produced as a result of tumor cells killed by NK cells	(27, 29)

Figure 1: ***Estimated mouse parameters.*** *See Table 1 in de Pillis [2].*

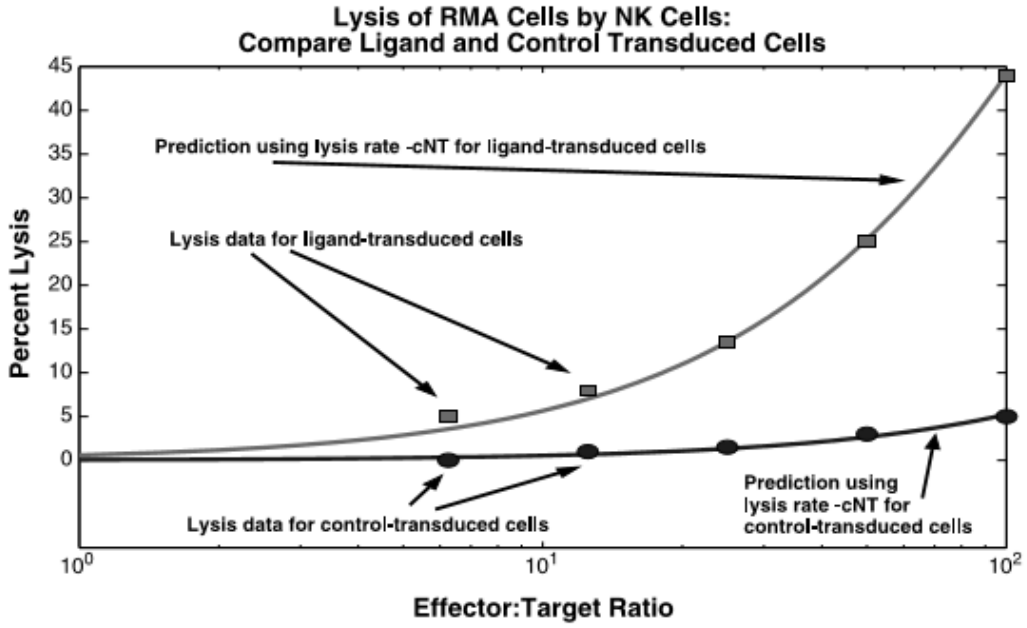

Figure 2: ***NK cell lysis.*** *This graph from [2] shows mathematical predictions from the model (smooth curves) plotted against actual experimental (squares and circles). The shallow curve predicts lysis percentages for control cells, whereas the steep curve predicts percentages for the ligand-transduced cells.*

effector/target lysis data with ligand and control transduced cells is graphed with the NK competition term. The model accurately produces a simulation of experimental interaction of NK and tumor cells so the power competition term is sufficient for representing NK/tumor lysis.

The same graphical analysis for the T-cell competition term does not show the same accuracy. Instead, the experimental data fit with curves produced by the rational forms found in Eq. (4). Figure 3 (top) shows four plots where the left two represent the model plotted with the T-cell lysis data that is control transduced and the right two show the T-cell lysis data that is ligand transduced. Each set of data is plotted with the power model and the rational model. The plot in Figure 3, at the bottom, shows a comparison of numerical error between the two model predictions. In the control transduced lysis data, either competition term accurately portrays the data, but in the ligand transduced data, the rational model has significantly less error than the power model. This data fitting experiment showed that the rational model shown in Eq. (4) provided the right model for

the T-cell/tumor lysis. The s parameter in Eq (4) represents the steepness of the curve, the λ term shows how lysis rate depends on effector/target ratio, while the parameter d is the maximum lysis rate of the T-cells.

The rational model in Eq (4) is known as phenomenological because it models observable outcomes and not direct underlying mechanisms. Because of this, the rational model was further analyzed using a similar data fitting experiment, but this time using the human CD8+ T-tumor lysis data. Figure 4 shows the results of the comparison of the power model with the rational model looking at two patients data. The top graph shows the power model predictions and it is easily seen that the model does not fit the data. The bottom graph, showing the rational model plotted with the same patient data, accurately predicts cell lysis for the human data. This further validates the need for the rational model.

The rational form of the competition term for CD8+ T-tumor lysis is established, so the sensitivity of the parameters in the model were estimated. The data from patient 9 was closely examined and each parameter was perturbed from its estimate value by 1 percent. Then the percent change in final tumor volume was calculated. The parameter sensitivity analysis shown in Figure 5 shows the system to be most sensitive to λ, the exponent in Eq (4), and to tumor growth variable a. The growth variable a represents tumor growth rate so it makes sense that the model will have different predictions based on tumor aggressiveness. The sensitivity in λ shows small changes in cytolytic effectiveness of tumor specific T-cells can effect clinical outcome. Then, treatment aggression is key for successful tumor targeting. Because sensitivity is low for the NK competition rate, c, then the NK population does not determine tumor size and should be considered with CD8+ T cell lysis. Before the mathematical model is tested under different conditions, the effectiveness of the immune system controlling ligand-transduced cells versus control transduced cells is evaluated. Figure 6 (top right) shows the effect of ligand-tranduced cells on the immune system response. The immune system is successful in controlling tumor cell population under these conditions, even when there is a rechallenge at day 10 with control transduced cells. Figure 5 (top left) shows that control transduced tumor cells escape the immune response with further aggression after the day 10 rechallenge. Therefore, the ligand transduced data is used in the proceeding simulations to create the best results. Using a computational solution to the mathematical model, three simulations are performed and solutions observed in Figure 7. The mathematical system is challenged with three different levels of tumor cells (10^4, 10^5, and 10^6). We reproduce the results of these simulations in Figure 8 using tumor cell population instead of mean surface area of tumor. Comparing the graphs in Figure 7 to the corresponding graphs in Figure 8, the same behavior is observed for the simulation with both CD8+ T-cells and NK cells and the simulation with no

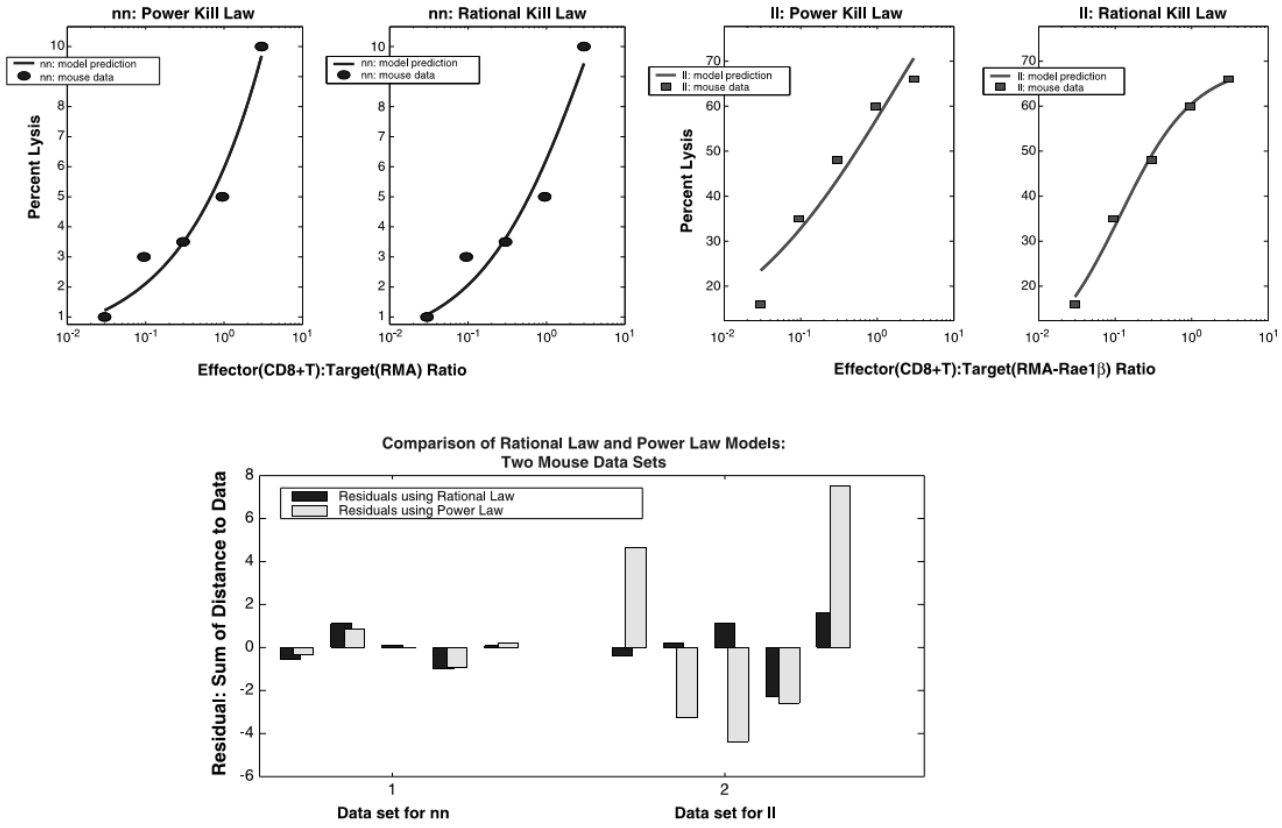

Figure 3: ***Comparison of competition term models (power versus rational).*** *Top, CD8+ T-tumor cell lysis. This row of graphs from [2] plots experimental data points (squares and circles) against mathematical cell lysis predictions (solid lines). The two graphs on the left plot the power model prediction and rational model prediction against lysis data for control transduced tumor cells. The two graphs on the right plot the power model prediction and rational model prediction against lysis data for ligand transduced tumor cells. Bottom, the bar chart on the bottom, plots the residuals (errors) for the same data sets (CD8+ T-cell lysis of control transduced and ligand transduced tumor cells). The height of each bar shows the value predicted by the power and rational models, minus the experimental data values at each effector/target ratio point. The difference between the power and rational models is most pronounced in the ligand transduced case, where effector cells are far more efficient at lysing tumor cells.*

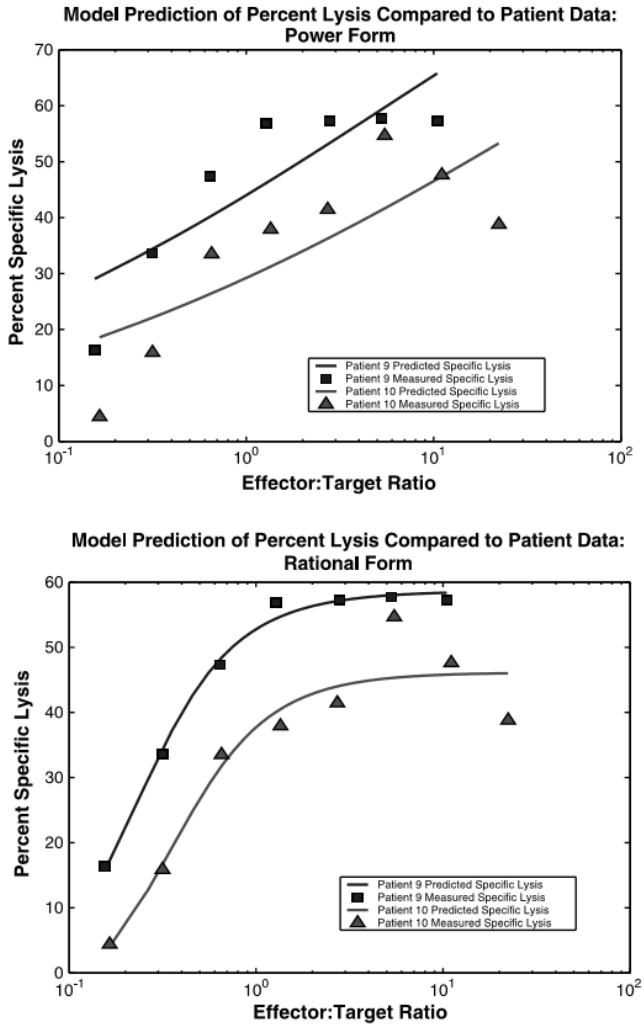

Figure 4: ***Model validation using human data.*** *In each graph (from [2], two separate simulations are plotted along with experimental data from two patients who experienced regression of melanoma. The model predictions are represented by the smooth curves, the squares represent patient 9, and the triangles represent patient 10. The top graph shows model predictions using the power model while the bottom graph shows model predictions using the rational model. Again, the rational model for predicting CD8+ T-tumor lysis rates provides a better fit to the experimental data than the power model.*

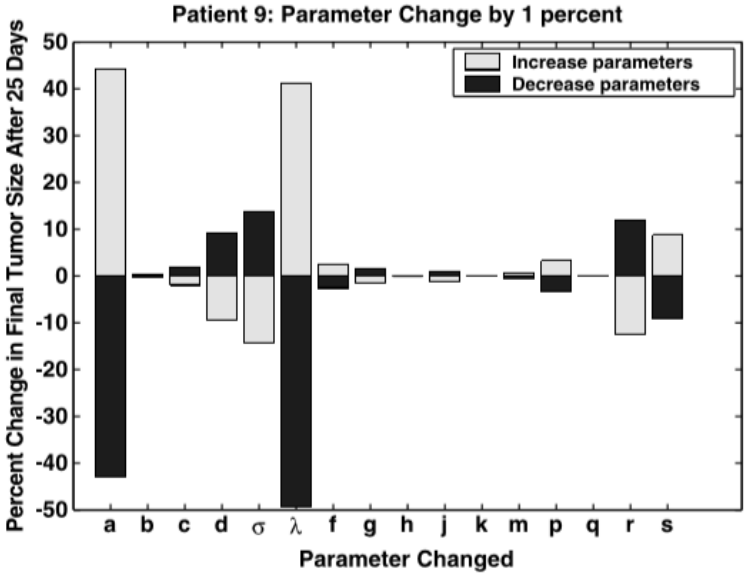

Figure 5: ***Sensitivity Analysis.*** *The model predicts that tumor size is the most effected by the CD8+ T-cell lysis variable, λ, and the growth rate of the tumor, a.*

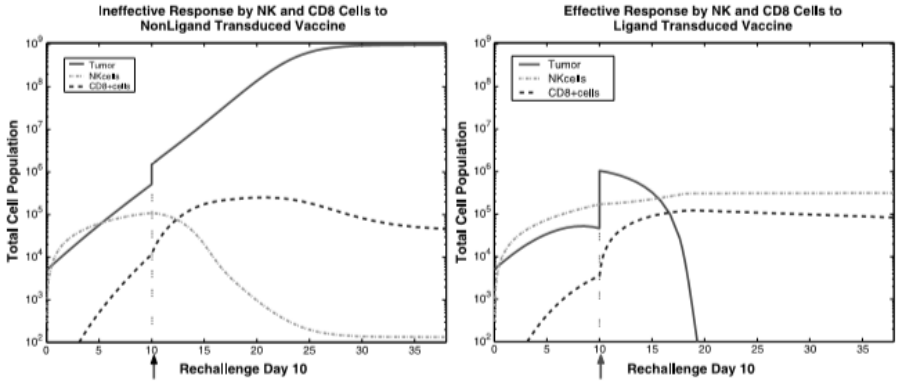

Figure 6: ***Ligand vs. control transduced in [2].*** *The top two graphs show the immune system response to ligand transduced tumor cells and control transduced tumor cells. The top right graph shows that the immune system is able to control the ligand transduced tumor cells while the top left shows that the immune system does not contain tumor cell growth of control tranduced cells. Both are rechallenged with control transduced cells on day 10.*

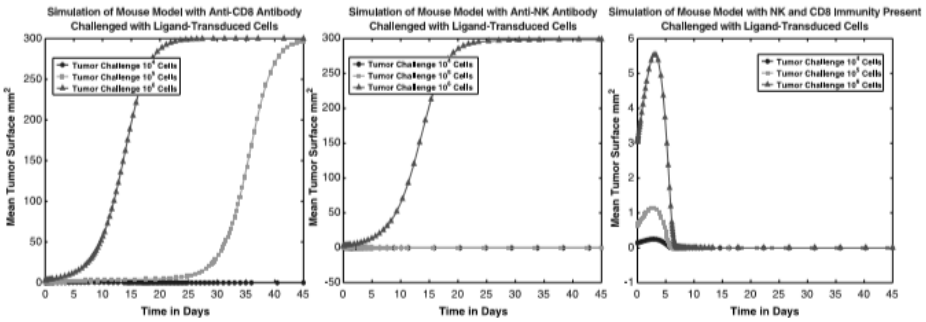

Figure 7: ***Simulations of model in [2].*** *The three graphs show three situations of the model starting with* 10^4, 10^5, *and* 10^6 *tumor cells. The left graph simulates the immune response without CD8+ T-cells and is only able to control tumor cell population starting at* 10^4. *The center graph shows the immune response without NK cells and can control tumor cell population starting at* 10^4 *and* 10^5.*The bottom right shows the immune response with both NK and CD8+ T cells and can control tumor cell population at all starting values of tumor cells.*

CD8+ T-cells. However the no NK cell simulation shows dramatic disagreement between their data and our reproduction of the graph.

Figure 7 (left) and Figure 8 (top) show the tumor growth in response to these three initial levels of tumor cells in the absence of CD8+ T-cell response. The system shows immune control for 10^4 initial tumor cells, but not for 10^5 or 10^6 initial tumor cells.

Figure 7 (center) and Figure 8 (center) show immune response to all three starting values of tumor cells with lack of NK cells instead of lack of CD8+ T-cells. The two graphs do not show the same result. Figure 7 (center) show depleting tumor cells starting at a challenge of 10^4 and 10^5 cells, but the immune cells still cannot destroy the tumor cell population when starting with 10^6 tumor cells. Figure 8 (center), the graph that we created, shows all three values of tumor cells uncontrolled by the immune system with lack of NK cells. This discrepancy could be caused from different starting values of CD8+ T-cells, but this is unlikely since T-cell values should start close to 0 (they are only recruited when tumor cells are present). There could also be an assumption in their data or model that we could not find and therefore did not account for.

Figure 7 (right) and Figure 8 (bottom) show the system with both NK cells and CD8+ T-cells present. This models a fully functioning immune system. The immune cells are now able to control tumor cells starting with a challenge of 10^4, 10^5, and 10^6 cells.

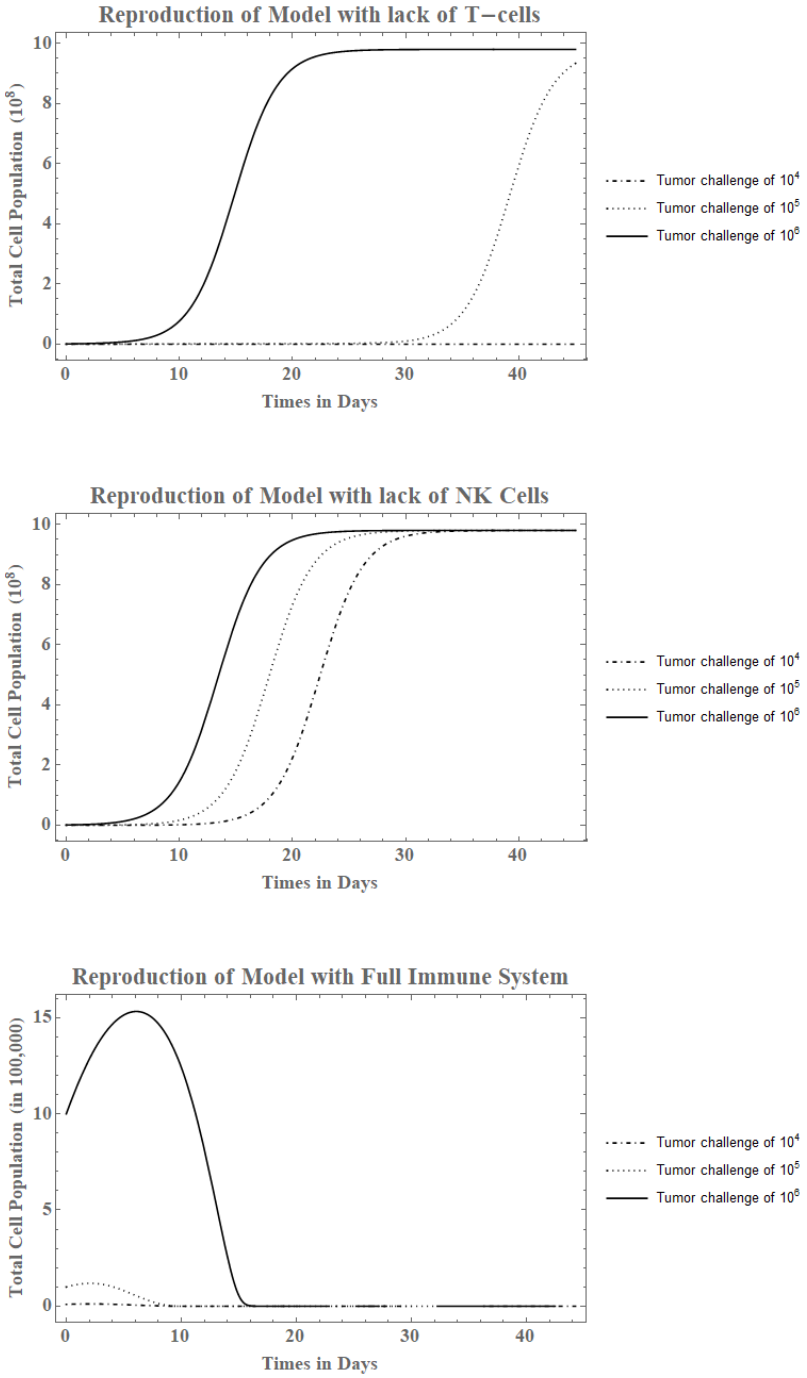

Figure 8: ***Reproduction of model****. The top graph simulates the immune system without CD8+ T-cells and also controls tumor growth for* 10^4*, but not* 10^5 *or* 10^6*. The center graph simulates the immune system without NK cells, but does not show the same results as Figure 8. In this instance the absence of NK cells produces an inability to control tumor cells at all three starting points in the immune system. The bottom graph simulates a fully functional immune system with all values of tumor cells being controlled.*

4. Further Analysis

The model shown is highly nonlinear so standard analytic techniques are not plausible. However, analyzing the model with specific cases could give us further insight. Consider the two cases where (i) the tumor cell population is significantly larger than the CD8+ T-cell population and (ii) the CD8+ T-cell population is significantly larger than the tumor cell population.

(i) We assume that the tumor cell population is significantly larger than the T-cell population, i.e. $T >> L$. This implies $L/T \approx 0$ and so we adopt the approximation

$$D = \frac{d\left(\frac{L}{T}\right)^{\lambda}}{s + \left(\frac{L}{T}\right)^{\lambda}} T \approx \frac{d\,(0)^{\lambda}}{s + (0)^{\lambda}} T = 0$$

Therefore, comparatively large amounts of tumor cells to T-cells result in the T-cell/tumor cell competition term (D) to disappear. This results in an slightly different system where the equations are:

$$\frac{dT}{dt} = aT\,(1 - bT) - cNT \tag{5}$$

$$\frac{dN}{dt} = \sigma - fN + \frac{gT^2}{h + T^2} N - pNT \tag{6}$$

$$\frac{dL}{dt} = -mL - qLT + rNT \tag{7}$$

When the solution of the new system is plotted with the same initial challenge of 10^4, 10^5, and 10^6 tumor cells, the results show that only the 10^4 tumor cell challenge is controlled by immune system defenses. This can be seen in Figure 9 as 10^5 and 10^6 tumor cell populations are uncontrolled by the solution. This is expected since there is no T-cell/tumor cell competition term in the tumor equation and there is no recruitment of T-cells within the T-cell equation. These factors lead to the tumor cell population growing without check when tumor cell population starts out efficiently high. Another interesting aspect about this solution is that Figure 9 is identical to the results of Figure 8 (top), which is the original model with lack of T-cells. This implies that T-cell effectiveness is based on the amount of recruitment of cells and the direct impact that the T-cells have on tumor population. Without the competition term, the T-cells are exactly as effective as they would be if they were not present in the system.

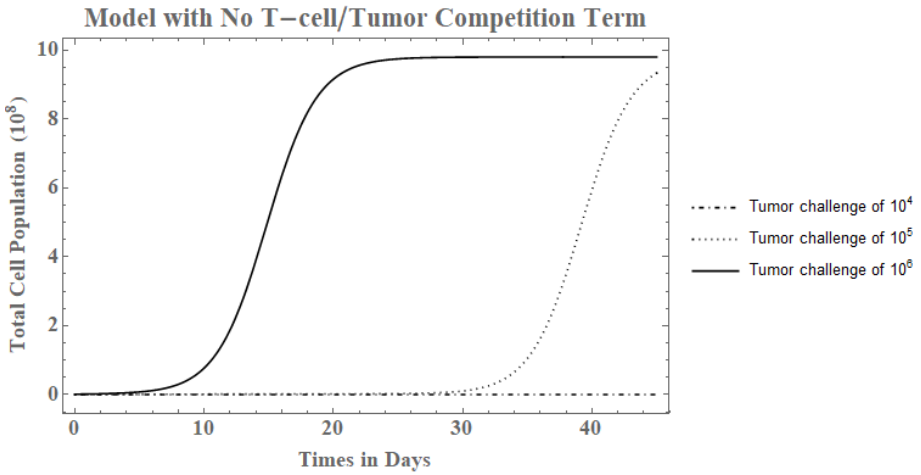

Figure 9: ***Model with no T-cell/tumor competition term****. The graph shows the system with the competition term eradicated. The immune system controls the growth for* 10^4*, but the challenge of* 10^5 *and* 10^6 *escapes the immune system defenses.*

(ii) Now, we assume that the T-cell population is significantly larger than the tumor population, i.e. $L >> T$. This implies $\frac{s}{L/T} \sim 0$ so we will take D to be

$$D = \frac{d\left(\frac{L}{T}\right)^{\lambda}}{s + \left(\frac{L}{T}\right)^{\lambda}} T = \frac{d}{\left(\frac{s}{\left(\frac{L}{T}\right)^{\lambda}} + 1\right)} T \approx d\,T$$

Large amounts of T-cells compared to tumor cells result in a T-cell/tumor competition term that is constant. This constant term relies on saturation level of tumor cell kill by T-cells (d) and by the tumor cell population (T). This new assumption does not change Eq. 1, Eq. 2, or Eq. 3, but only the D term.

When we solve the new system we use the same challenge of T-cells (10^4, 10^5, and 10^6) and leave the constant D term with $T = 10^4$ and $d = d(ln)$, see Figure 1 for value. Figure 10 shows that a system with constant T-cell/tumor competition term controls challenges of 10^4 and 10^5, but is unable to defend against the 10^6 challenge. With large amount of T-cells we would expect the immune system would be able to control tumor population more than with large amounts of tumor and Figure 10 confirms this intuition.

5. Discussion

Phenomenologically, the data fitting experiments in [2] suggest that the rational form of the competition term is the most accurate at modeling the interaction of

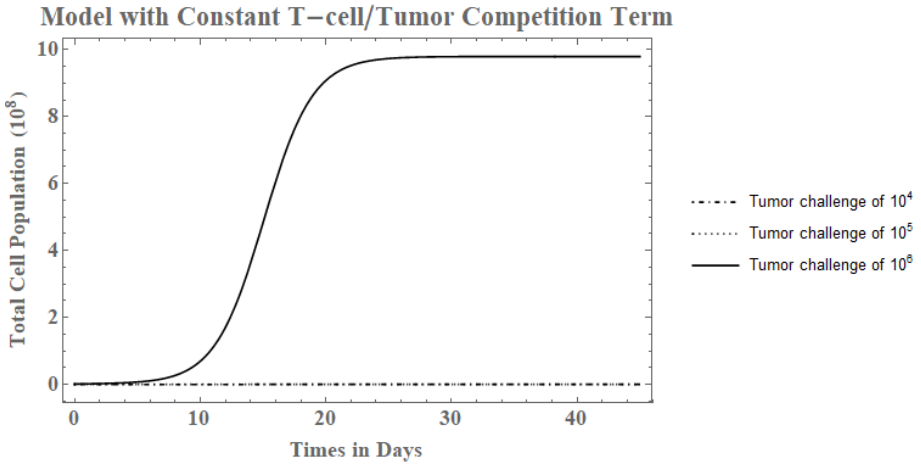

Figure 10: ***Model with constant T-cell/tumor competition term.*** *The graph shows the system with the competition term constant. The immune system controls the growth for* 10^4 *and* 10^5 *tumor cells, but the* 10^6 *challenge escapes the immune system defenses.*

the T-cells and tumor cells. The competition term between NK and tumor cells show the proportional effects of NK cells to both NK cell population and tumor cell population. Further research into the underlying biological significance to why the rational form of the competition term for T-cells fits the tumor cell data could reveal a immunological significance to T-cell specific treatments. Finding a mathematical model that fits the empirical data gives insight to how the immune system responds and tracks ways that could be effective in manually targeting tumors.

This current model does not account for all the immune system defenses, but the fact that it fits the empirical data suggests that it can represent immune response data. The simulations with the model in [2] suggest that the effect of CD8+ T-cells should be of focus and may be more effective in immunology. However, the reproduction of the simulations we created show that tumor cell population grows at any starting supply in the absence of NK cells which implies that NK cells may be the more effective immune defense cells against tumor cells. In either case, further studies of NK and T-cell dynamics could supply information on which immune defense to utilize to fight tumor cells.

Making the assumption that tumor cell population vastly exceeds T-cell population, we see the eradication of the T-cell/tumor competition term and two of the three challenges of tumor grow immensely. The smaller challenge is likely controlled by the remaining defenses of the NK cells. The results of this assumption also mirrors the system with no T-cells present, therefore showing that the competition term is necessary for T-cell effectiveness. We also found that if T-cell

population exceeded tumor population by a great number, that the competition term would stay at a constant value dependent on tumor population. Now, only the highest challenge of tumor could not be lysed by the immune system showing that the constant competition term is the most effective system besides the full immune system. This is expected because we are assuming the T-cell population is large. No direct applications to immunotherapy can be found in the results of the model, however the fact the model fits experimental data shows that this model can accurately model immune defenses. A study of why this model can represent the data could lead to significant application to immunotherapy and give insight into which cells are the most effective at defending the body and killing cancerous cells.

Acknowledgments

I would like to thank Dr. Richard Cangelosi, Assistant Professor of Mathematics, Gonzaga University, for his guidance with this project.

References

[1] (2017). Cancer Prevention and Control *Centers for Disease Control and Prevention* CDC-INFO: Atlanta, GA.

[2] de Pillis, Lisette G., Radunskaya, Ami E. and Wiseman, Charles L. (2005). A Validated Mathematical Model of Cell-Mediated Immune Response to Tumor Growth. *Cancer Res*, **65**(17): 7950-7958.

[3] Strogatz, Steven H. (2015). *Nonlinear Dynamics and Chaos with Applications to Physics, Biology, Chemistry, and Engineering*. Westview Press: Boulder, CO.